

# Node Power Injection Modification Model Based on Direct Derivation for Lossy Power Flow in Hybrid AC-DC Distribution Networks

Hao Wang, Changzheng Shao, *Member, IEEE*, Yu Wang, *Member, IEEE*, Bo Hu, *Member, IEEE*, Kaigui Xie, *Senior Member, IEEE*, and Pierluigi Siano, *Senior Member, IEEE*

**Abstract**—Lossy power flow naturally extends lossless linear power flow to lossy distribution networks, further improving the accuracy of approximate computation and analysis. However, these enhanced versions are only applicable at the alternating current (AC) transmission level, and the accuracy is limited in distribution networks, especially in hybrid AC-direct current (DC) distribution networks. In this paper, we revisit the lossy power flow model and extend it to hybrid AC-DC distribution networks with multi-terminal voltage source converters. The proposed lossy power flow model can be reformulated as an iteration problem with node power injection as the fixed point. For this purpose, a node power injection modification model based on direct derivation is proposed by exploiting the negligibility of the phase angle differences, and iteratively solving lossy power flows for both AC and DC sub-networks. For coupling devices, to guarantee that the power flow is matched on both AC and DC sides, we formulate a rigorous fixed-point problem to solve the lossy power flow of voltage source converters. Finally, the high accuracy and computational efficiency of the proposed model are verified on multiple test cases.

**Index Terms**—Hybrid AC-DC distribution network, voltage source converter, lossy power flow, node power injection.

## NOMENCLATURE

### A. Sets and Indices

$\kappa, \bar{\kappa}$  Set of all branches (edges) in a node for alternating current (AC) and direct current (DC) distribution networks

$\ell$  Set of all voltage source converters

$\ell_{ma}$  Set of all master voltage source converters under master-slave control

$\ell_{sl}$  Set of all slave voltage source converters under master-slave control

$\ell_{dp}$  Parallel set of all voltage source converters under droop control

$i$  Node index for AC or DC distribution networks,  $i = \{1, 2, \dots, N\}$

$l$  Voltage source converter index,  $l = \{1, 2, \dots, L\}$

$\mathcal{L}$  Set of all  $PQ$  nodes for AC distribution networks

$\mathcal{N}$  Set of all nodes for AC or DC distribution networks

$\mathcal{R}$  Set of all slack nodes for AC distribution networks

$\mathcal{S}$  Set of all  $PQ$  and  $PV$  nodes for AC distribution networks

$\mathcal{T}$  Set of all  $PV$  and slack nodes for AC distribution networks

### B. Parameters

$\delta$  Convergence coefficient

$a, b, c$  No-load, linear, and quadratic coefficients of converter loss conductance and susceptance

$C_1, C_2$  Constant matrices composed of conductance and susceptance elements for AC networks

$\bar{g}_{ij}$  The  $(i-j)^{\text{th}}$  element of conductance matrix  $\bar{G}$  for DC distribution networks

$g_{l/c}, b_{l/c/f}$  Equivalent conductance and susceptance of each element of converter station (transformer, phase shifter, and filter)

$It_{\max}$  The maximum number of iterations

$N$  Dimension of variable

$pol$  Number of electrodes in DC distribution networks, taking 1 for unipolar and 2 for bipolar

$x$  Number of external iterations

$\bar{x}, \bar{x}$  Numbers of internal iterations for AC and DC distribution networks

$y_{ij}$  The  $(i-j)^{\text{th}}$  element of admittance matrix  $Y = G + jB$  for AC distribution networks,  $y_{ij} = g_{ij} + jb_{ij}$

$Z_{c,l}$  Impedance of phase reactor of the  $l^{\text{th}}$  VSC

### C. Variables

$\theta_i$  Voltage angle for AC distribution networks at

Manuscript received: February 10, 2024; revised: May 11, 2024; accepted: July 17, 2024. Date of CrossCheck: July 17, 2024. Date of online publication: August 7, 2024.

This work was supported by the National Natural Science Foundation of China (No. 52022016).

This article is distributed under the terms of the Creative Commons Attribution 4.0 International License (<http://creativecommons.org/licenses/by/4.0/>).

H. Wang, C. Shao, Y. Wang, B. Hu, and K. Xie (corresponding author) are with State Key Laboratory of Power Transmission Equipment Technology, Chongqing University, Chongqing 400044, China (e-mail: wanghao@cqu.edu.cn; cshao@cqu.edu.cn; yu\_wang@cqu.edu.cn; hboy8361@163.com; kaiguixie@vip.163.com).

P. Siano is with the Department of Management and Innovation Systems, University of Salerno, Fisciano 84084, Italy, and he is also with the Department of Electrical and Electronic Engineering Science, University of Johannesburg, Johannesburg 2006, South Africa (e-mail: siano.pierluigi@gmail.com).

DOI: 10.35833/MPCE.2024.000059



	node $i$
$\theta_{f,l}$	Voltage phase angle of filter for the $l^{\text{th}}$ VSC
$\theta_{fc,l}$	Voltage phase angle difference between filter and phase reactor of the $l^{\text{th}}$ VSC
$\theta_{sf,l}$	Voltage phase angle difference between transformer and filter of the $l^{\text{th}}$ VSC
$\Delta f_{P,l}$	Mismatch of active power of the $l^{\text{th}}$ VSC
$\Delta f_{Q,l}$	Mismatch of reactive power of the $l^{\text{th}}$ VSC
$f(x_i)$	Result calculated using different approximation methods
$\bar{P}_i$	Power injection for DC distribution networks at node $i$
$\bar{P}_{dc,l}$	Power injection from the $l^{\text{th}}$ converter into DC distribution network
$\bar{P}_i^{\text{ls}}$	Power injection at DC node $i$ for the $x^{\text{th}}$ iteration
$\tilde{P}_i + j\tilde{Q}_i$	Complex power injection for AC distribution networks at node $i$
$\tilde{P}_i^{\text{ls}}, \tilde{Q}_i^{\text{ls}}$	Active and reactive power injections at AC node $i$ for the $x^{\text{th}}$ iteration
$\tilde{P}_{c,l}, \tilde{Q}_{c,l}$	Active and reactive power injections through the $l^{\text{th}}$ converter
$\tilde{P}_{s,l}, \tilde{Q}_{s,l}$	Active and reactive power injections from converters into AC distribution network at the $l^{\text{th}}$ point of common coupling (PCC) node
$\tilde{P}_{cf,l}, \tilde{Q}_{cf,l}$	Active and reactive power flows of transformer for the $l^{\text{th}}$ converter
$\tilde{P}_{sf,l}, \tilde{Q}_{sf,l}$	Active and reactive power flows of phase shifter for the $l^{\text{th}}$ converter
$\overline{PL}_{ij}$	Total loss for DC branch $i-j$
$\overline{PL}_{ij}^i$	Virtual demand allocated to DC node $i$ to compensate loss of branch $i-j$
$\widetilde{PL}_{\text{vsc},l}$	Active loss for the $l^{\text{th}}$ converter
$\widetilde{PL}_{ij}, \widetilde{QL}_{ij}$	Active and reactive power losses for AC branch $i-j$
$\widetilde{PL}_{ij}^i, \widetilde{QL}_{ij}^i$	Active and reactive power demands allocated to AC node $i$ to compensate loss of branch $i-j$
$\tilde{Q}_{f,l}$	Reactive power injection through filter for the $l^{\text{th}}$ converter
$\tilde{U}_{f,l}$	Voltage magnitude of filter for the $l^{\text{th}}$ converter
$\tilde{U}_{c,l}, \theta_{c,l}$	Voltage magnitude and phase angle for the $l^{\text{th}}$ converter
$\tilde{U}_{s,l}, \theta_{s,l}$	Voltage magnitude and phase angle at the $l^{\text{th}}$ PCC node
$\tilde{U}_i, \bar{U}_i$	AC and DC voltage magnitudes at node $i$
$Y_i$	Result calculated using standard iterative method

## I. INTRODUCTION

**H**YBRID alternating current (AC)-direct current (DC) distribution networks combine the advantages of both AC and DC architectures, facilitating the integration of renewable energy sources as well as the access of DC loads (e.g., electric vehicles) [1], [2], and also enhancing the flexibility of system-level regulation. Their main feature is the combination of both AC and DC networks in the same distri-

bution network, and the key link for achieving this is the voltage source converter (VSC). Different forms of AC-DC interconnections such as point-to-point and multi-terminal (MT) can be constructed using these flexible coupling devices. Virginia Tech launched the ‘‘Sustainable Building Initiative (SBI)’’ program and the ‘‘Sustainable Building and Nanogrids (SBN)’’ project, in which a hybrid AC-DC grid operation structure was proposed based on hierarchical interconnection [3]. Elenia Oy, a Finnish company, replaced the original medium-voltage lines with low-voltage DC distribution network in rural areas, facilitating the integration of distributed generation and energy storage with good application prospects [4]. The first fully controllable power electronic flexible substation has been built in Zhangbei Demonstration Area, in China, which can ensure the bidirectional input and output at four voltage levels, i.e., 10 kV AC,  $\pm 10$  kV DC, 750 V DC, and 380 V AC, and can flexibly connect renewable energy sources and AC or DC loads [5]. The DC distribution network in Suzhou, China, has three voltage levels, i.e.,  $\pm 10$  kV, 750 V, and 375 V, which ensures multi-level integration of photovoltaic power generation and high-quality power supply for different residents [6].

Given that hybrid AC-DC distribution networks offer unique capability in regulating power flow, the power flow problem of hybrid AC-DC distribution networks is becoming an urgent research task. Considering the increasing scale of hybrid AC-DC distribution networks, the computational complexity of the traditional nonlinear iteration methods, i.e., sequential methods [7]-[10] and unified methods [11]-[15], is severely challenged. The linear power flow (LPF) model [16]-[19] aims to linearize the nonlinear power flow equations, which has the advantages of computational simplicity and ease of being embedded into optimization models [20]-[22], and can effectively reduce the computational complexity and avoid convergence difficulties. However, neglecting resistive losses is recognized as one of the largest sources of error in these models. In addition, with the increase in the scale and capacity of distributed renewable energy sources, the problems of voltage fluctuation and excessive network losses are becoming more and more prominent, further amplifying the disadvantages of the above methods. In contrast, the lossy power flow model [23] refers to dynamically adjusting the node power injection by adding losses and updating the solution to a new set of operating points to re-solve the LPF model. The technique is formulated as a fixed-point iteration problem with respect to node power injection, and provides a better approximation of the actual operating state of the distribution network. Consequently, the lossy power flow is an enhanced version of the lossless LPF, and is one of mainstream methods for approximate computation and analysis.

Currently, lossy power flow models can be divided into DC power flow and decoupling AC LPF models. A series of novel DC power flow models incorporating losses have been proposed in [23]-[26], as is done in the so-called  $\alpha$ -matching method. The iteration process of these models begins from a known power flow solution, and compensates the approximate losses calculated from the known solution to the power

injection at the corresponding node. However, these models only focus on active power losses, and ignore voltage magnitude and reactive power, which can be a fatal in hybrid AC-DC distribution networks, because the power flow of VSC rely heavily on complete power flow information. Therefore,  $\alpha$ -matching method is extended to AC LPF models considering both active and reactive losses [27]-[30]. The difference between these models lies in the formulas for estimating the losses, e.g., the losses are modeled as a quadratic function of the current (or branch flow) in [27] and [28], while the losses are modeled as a nonlinear function of the voltage in [29] and [30]. The former is a simplified expression of the later, thus the loss estimation is less accurate. In summary, such lossy models that heuristically incorporate losses have the same drawbacks: ① the estimation of the losses depends on the current iteration of the solution, resulting in relatively conservative performance of error correction; ② branch losses must be explicitly computed during iterations to modify power injection, adding an extra computational burden; ③ the assumptions in the modeling are supported in transmission networks with long transmission lines [23], [25] and low resistance-to-reactance ( $r/x$ ) ratios [31], [32], but will be violated in distribution networks, especially for hybrid AC-DC distribution networks.

Another shortcoming of the existing research works is that lossy power flow models can only serve pure AC or pure DC distribution networks, but are difficult to be directly integrated into hybrid AC-DC distribution networks. Developing an accurate LPF for the lossy power flow of VSC is a great challenge [33]. For VSC based multi-terminal direct current (MTDC) meshed AC-DC distribution networks, an LPF algorithm is proposed in [34] with VSC losses; however, the nonlinearity of VSC is preserved in the calculation. Reference [35] investigates the optimal power flow problem for HVDC transmission network, and although some robust models are provided, all of them retain the nonlinearity of the VSC. To avoid solution challenges caused by nonlinearity, the power losses of VSC are neglected in models such as reliability evaluation [36] and post-disaster restoration [37], which may bring large errors. Therefore, a wide variety of formulas are proposed in [38] for the optimal power flow of hybrid AC-DC distribution networks, including a detailed linear approximation of the VSC. However, these models are derived based on direct current power flow (DCPF) assumptions (e.g.,  $U \approx 1$  p.u.,  $\sin \theta \approx \theta$ ), and cannot accurately approximate the reactive power and voltage magnitude. In fact, the steady-state operation of the VSC is very dependent on the reactive power and voltage magnitude, thus these models reduce the regulation capability of the VSC and are less applicable. In conclusion, the simplified VSC power flow model not only fails to accurately quantify its own operating state, but also further amplifies the errors of the connected AC and DC nodes, leading to a large deviation in the power flow results of the entire DC distribution network.

To fill these research gaps, this paper investigates methods to enhance the potential of lossy power flow model for hybrid AC-DC distribution networks. The contributions of this paper are summarized as follows.

1) A novel lossy power flow model is proposed for hybrid AC-DC distribution networks, including AC sub-networks, DC sub-networks, and VSCs. The model fully follows the sequential algorithmic framework and supports multiple types of AC-DC interconnections, and allows for the integration of renewable energy sources. The accuracy and computational efficiency of the model are improved to different degrees in different scale test cases, and it shows excellent generalization and robustness.

2) At the system level, the proposed lossy power flow model is reformulated as a novel fixed-point problem related to node power injection. Taking advantage of the negligible phase angle of the distribution network, a fixed-point modification model based on direct derivation is proposed, which requires only known voltage magnitude to modify the node power injection without explicit estimation of losses.

3) At the device level, a rigorous fixed-point formulation of the lossy power flow is developed based on the complete AC equivalent circuit, which efficiently solves the power mismatch problem on both the AC and DC sides. The proposed model requires fewer assumptions to accurately solve all the power flow information and improves the power regulation capability of the VSC.

The remainder of this paper is organized as follows. Section II presents the proposed lossy power flow model. The standard lossless LPF model for AC and DC distribution networks is reviewed, and the AC lossy power flow model based on an improved fixed-point modification formulation is derived and extended to DC distribution networks. Section III introduces the lossy power flow model for VSC in detail and declares the algorithmic framework for hybrid AC-DC networks. Extensive comparisons of the proposed model with existing models on several modified test systems are performed in Section IV. Section V concludes and points to future research.

## II. PROPOSED LOSSY POWER FLOW MODEL FOR AC AND DC DISTRIBUTION NETWORKS

### A. Standard Lossless LPF Model for AC and DC Distribution Networks

The matrix form of the standard lossless LPF model [16] for the AC distribution network can be detailed by:

$$\begin{cases} \begin{bmatrix} \tilde{\mathbf{P}}_S \\ \tilde{\mathbf{Q}}_L \end{bmatrix} + \mathbf{C}_1 \begin{bmatrix} \boldsymbol{\theta}_R \\ \tilde{\mathbf{U}}_T \end{bmatrix} = \mathbf{C}_2 \begin{bmatrix} \boldsymbol{\theta}_S \\ \tilde{\mathbf{U}}_L \end{bmatrix} \Rightarrow \begin{bmatrix} \tilde{\mathbf{P}} \\ \tilde{\mathbf{Q}} \end{bmatrix} = \boldsymbol{\Phi}_{AC} \left( \begin{bmatrix} \boldsymbol{\theta} \\ \tilde{\mathbf{U}} \end{bmatrix} \right) \\ \mathbf{C}_1 = \begin{bmatrix} \mathbf{B}'_{SR} & -\mathbf{G}_{ST} \\ \mathbf{G}_{LR} & \mathbf{B}_{LT} \end{bmatrix} \\ \mathbf{C}_2 = -\begin{bmatrix} \mathbf{B}'_{SS} & -\mathbf{G}_{SL} \\ \mathbf{G}_{LS} & \mathbf{B}_{LL} \end{bmatrix} \end{cases} \quad (1)$$

where  $\tilde{\mathbf{P}}$  and  $\tilde{\mathbf{Q}}$  are the vectors of active and reactive power injections at AC node, respectively;  $\tilde{\mathbf{U}}$  and  $\boldsymbol{\theta}$  are the vectors of voltage magnitude and voltage phase angle at AC node, respectively;  $\mathbf{B}'$  is the susceptance matrix  $\mathbf{B}$  without shunt elements; and  $\boldsymbol{\Phi}_{AC}(\cdot)$  is the mathematical notation for linear power flow in the AC distribution network, and the specific formula can be found in [16]. Similarly, the standard lossless

LPF model for the DC distribution network can be formulated in vector form as:

$$\bar{\mathbf{P}} = \bar{\mathbf{G}}\bar{\mathbf{U}} \Rightarrow \bar{\mathbf{P}} = \Phi_{\text{DC}}(\bar{\mathbf{U}}) \quad (2)$$

where  $\bar{\mathbf{P}}$  is the vector of active power injections at DC node;  $\bar{\mathbf{U}}$  is the vector of voltage magnitude at DC node;  $\bar{\mathbf{G}}$  is the conductance matrix of the DC line; and  $\Phi_{\text{DC}}(\cdot)$  is the mathematical notation for linear power flow in the DC distribution network. Detailed derivations of (1) and (2) are given in Supplementary Material A. The lossless power flow model expressed by (1) and (2) is linear, but ignores the network losses since it assumes that the absolute values of the sending and receiving flows are equal for each branch. In other words, the imbalance of the node power injection is not evenly distributed to the corresponding nodes, but is all borne by the slack node, resulting in the power flow distribution deviating from the actual state.

### B. Lossy Power Flow Model Based on Direct Derivation for AC Distribution Networks

The lossy power flow model requires several iterations of the standard lossless LPF model for AC or DC distribution networks, which is mathematically defined as a fixed-point iteration problem with respect to node power injection, described by (1) (or (2)) and a fixed-point modification model. For this purpose, the branch losses are equated to the virtual demand with impedance  $Z_{\text{equ}}$  (or  $R_{\text{equ}}$  in the DC distribution network), and the equivalent load model is shown in Fig. 1, where the consumed power is numerically equal to 1/2 of the sum of all branch losses for a node. Then, the node injection can be modified by the node power balance equation, and the power flow can be re-solved by resubstituting the new operating point into (1) or (2). The above process is looped until the node power injection converges to a fixed point.

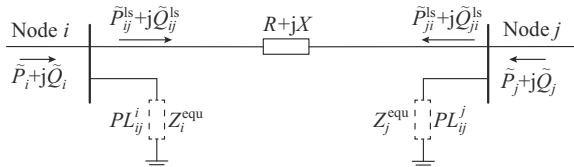


Fig. 1. Equivalent load model of branch losses for AC distribution network.

In AC distribution network, the total branch losses can be decoupled into active and reactive components, respectively:

$$\begin{cases} \widetilde{PL}_{ij} = \widetilde{PL}_{ij}^i + \widetilde{PL}_{ij}^j = g_{ij}[(\tilde{U}_i - \tilde{U}_j)^2 + (\theta_i - \theta_j)^2] \\ \widetilde{QL}_{ij} = \widetilde{QL}_{ij}^i + \widetilde{QL}_{ij}^j = -b_{ij}[(\tilde{U}_i - \tilde{U}_j)^2 + (\theta_i - \theta_j)^2] \end{cases} \quad (3)$$

To reduce the gap between (1) and the nonlinear benchmark, the branch losses should be allocated to the nodes  $i$  and  $j$ :

$$\begin{cases} \widetilde{PL}_{ij}^i = g_{ij}[(\tilde{U}_i - 1)(\tilde{U}_i - \tilde{U}_j) + \theta_i(\theta_i - \theta_j)] \\ \widetilde{QL}_{ij}^i = -b_{ij}[(\tilde{U}_i - 1)(\tilde{U}_i - \tilde{U}_j) + \theta_i(\theta_i - \theta_j)] \end{cases} \quad (4)$$

Here, node  $j$  is assumed to be a slack node, i.e., the voltage magnitude is 1 p.u. and the phase angle is 0. For proof of (4), refer to Supplementary Material B.

The  $r/x$  ratios are usually low for transmission lines, but this assumption may be violated in distribution networks. In addition, voltage phase angle differences of AC distribution networks are usually much smaller than those of AC transmission networks due to the fact that distribution lines are usually much shorter than transmission lines. Most of the phase differences on transmission lines are concentrated within  $\pm 30^\circ$  [16], [25]. However, on very long transmission lines, the phase angle difference can even reach  $40^\circ$  [23]. Therefore, the phase angle differences cannot be neglected in transmission networks for network loss approximation. In contrast, phase angle differences across distribution lines are generally much smaller, which is a widely recognized assumption in the academic community. Due to power quality standards, distribution networks are designed, where the voltages are close to nominal values under normal operation, i.e., magnitudes are within 0.9-1.1 p.u., phase angle differences are as small as possible, and a voltage imbalance factor is lower than 5% [39]. Based on the above facts, a typical distribution network is characterized by the following two features: ①  $x \gg r$  no longer holds, implying that the active and reactive branch losses are numerically closer; ② the phase angle differences are sufficiently small, implying that  $\tilde{U}_{ij}$  is greater than  $\theta_{ij}$ . In other words, the phase angle component of the losses is less than the voltage magnitude component. Consequently, the losses neglecting the phase difference can be approximated as [40]:

$$\begin{cases} \widetilde{PL}_{ij}^i \approx g_{ij}(\tilde{U}_i - 1)(\tilde{U}_i - \tilde{U}_j) \\ \widetilde{QL}_{ij}^i \approx -b_{ij}(\tilde{U}_i - 1)(\tilde{U}_i - \tilde{U}_j) \end{cases} \quad (5)$$

The node power injection depends not only on its own generation and real demand, but also on the virtual loads. Therefore, the lossy node power balance equation for the AC distribution network can be constructed as:

$$\begin{cases} \tilde{P}_i = \tilde{P}_i^G - \tilde{P}_i^D = \tilde{P}_i^{\text{ls}(0)} + \sum_{j \in \kappa} \widetilde{PL}_{ij}^{i(0)} = \\ \tilde{P}_i^{\text{ls}(1)} + \sum_{j \in \kappa} \widetilde{PL}_{ij}^{i(1)} = \dots = \tilde{P}_i^{\text{ls}(x)} + \sum_{j \in \kappa} \widetilde{PL}_{ij}^{i(x)} \\ \tilde{Q}_i = \tilde{Q}_i^G - \tilde{Q}_i^D = \tilde{Q}_i^{\text{ls}(0)} + \sum_{j \in \kappa} \widetilde{QL}_{ij}^{i(0)} = \\ \tilde{Q}_i^{\text{ls}(1)} + \sum_{j \in \kappa} \widetilde{QL}_{ij}^{i(1)} = \dots = \tilde{Q}_i^{\text{ls}(x)} + \sum_{j \in \kappa} \widetilde{QL}_{ij}^{i(x)} \end{cases} \quad (6)$$

where the superscripts G and D denote power generation and load demand, respectively; and the superscript symbol  $(x)$  denotes the number of iterations for lossy power flow. When  $x=0$ , there is no branch losses, so  $\tilde{P}_i^{\text{ls}(0)} = \tilde{P}_i$  for all PQ and PV nodes, and  $\tilde{Q}_i^{\text{ls}(0)} = \tilde{Q}_i$  for all PQ nodes.

On the other hand, the relationship between the linear approximation of the branch flow and the node power injection is formulated as:

$$\begin{cases} \tilde{P}_i^{\text{ls}} = g_{ii}\tilde{U}_i^2 + \sum_{j \in \kappa(i)} P_{ij}^{\text{ls}} \approx g_{ii}\tilde{U}_i^2 + \sum_{j \in \kappa} [g_{ij}(\tilde{U}_i - \tilde{U}_j) - b_{ij}(\theta_i - \theta_j)] \\ \tilde{Q}_i^{\text{ls}} = -b\tilde{U}_i^2 + \sum_{j \in \kappa(i)} Q_{ij}^{\text{ls}} \approx -b\tilde{U}_i^2 + \sum_{j \in \kappa} [-b_{ij}(\tilde{U}_i - \tilde{U}_j) - g_{ij}(\theta_i - \theta_j)] \end{cases} \quad (7)$$

For this purpose, it is assumed that the  $(x+1)^{\text{th}}$  solution  $[\tilde{\mathbf{U}}^{(x+1)}, \boldsymbol{\theta}^{(x+1)}]^T$  is known and substituted into (5) and (7) to yield the approximation of branch losses and power flows:

$$\begin{cases} \tilde{\mathbf{P}}_{ij}^{\text{ls}(x+1)} \approx \mathbf{g}_{ij}(\tilde{\mathbf{U}}_i^{(x+1)} - \tilde{\mathbf{U}}_j^{(x+1)}) - b_{ij}(\theta_i^{(x+1)} - \theta_j^{(x+1)}) \\ \tilde{\mathbf{Q}}_{ij}^{\text{ls}(x+1)} \approx -b_{ij}(\tilde{\mathbf{U}}_i^{(x+1)} - \tilde{\mathbf{U}}_j^{(x+1)}) - \mathbf{g}_{ij}(\theta_i^{(x+1)} - \theta_j^{(x+1)}) \end{cases} \quad (8)$$

$$\begin{cases} \tilde{\mathbf{P}}\tilde{\mathbf{L}}_{ij}^{i(x+1)} \approx \mathbf{g}_{ij}(\tilde{\mathbf{U}}_i^{(x)} - 1)(\tilde{\mathbf{U}}_i^{(x+1)} - \tilde{\mathbf{U}}_j^{(x+1)}) \\ \tilde{\mathbf{Q}}\tilde{\mathbf{L}}_{ij}^{i(x+1)} \approx -b_{ij}(\tilde{\mathbf{U}}_i^{(x)} - 1)(\tilde{\mathbf{U}}_i^{(x+1)} - \tilde{\mathbf{U}}_j^{(x+1)}) \end{cases} \quad (9)$$

Formula (9) can explain why the proposed lossy power flow model is able to compensate the losses more accurately to the corresponding node. If the known  $\tilde{\mathbf{U}}_i^{(x)}$  is substituted into (4), the losses can be easily estimated and allowed to modify the node injection. However,  $\tilde{\mathbf{U}}_i^{(x)}$  is not accurate and the effectiveness of error correction is relatively conservative. In this paper, (9) substitutes  $\tilde{\mathbf{U}}_i^{(x+1)}$  for  $\tilde{\mathbf{U}}_i^{(x)}$ , which is equivalent to modifying the node power injections in advance using the losses from the next iteration, allowing for predictive error correction. Substituting (7) - (9) into (6) yields:

$$\begin{cases} \mathbf{g}_{ii}\tilde{\mathbf{U}}_i^{2(x)} + \sum_{j \in \kappa} [\mathbf{g}_{ij}\tilde{\mathbf{U}}_i^{(x-1)}(\tilde{\mathbf{U}}_i^{(x)} - \tilde{\mathbf{U}}_j^{(x)}) - b_{ij}(\theta_i^{(x)} - \theta_j^{(x)})] = \\ \mathbf{g}_{ii}\tilde{\mathbf{U}}_i^{2(x+1)} + \sum_{j \in \kappa} [\mathbf{g}_{ij}\tilde{\mathbf{U}}_i^{(x)}(\tilde{\mathbf{U}}_i^{(x+1)} - \tilde{\mathbf{U}}_j^{(x+1)}) - b_{ij}(\theta_i^{(x+1)} - \theta_j^{(x+1)})] \\ -b_{ii}\tilde{\mathbf{U}}_i^{2(x)} + \sum_{j \in \kappa} [-b_{ij}\tilde{\mathbf{U}}_i^{(x-1)}(\tilde{\mathbf{U}}_i^{(x)} - \tilde{\mathbf{U}}_j^{(x)}) - \mathbf{g}_{ij}(\theta_i^{(x)} - \theta_j^{(x)})] = \\ -b_{ii}\tilde{\mathbf{U}}_i^{2(x+1)} + \sum_{j \in \kappa} [-b_{ij}\tilde{\mathbf{U}}_i^{(x)}(\tilde{\mathbf{U}}_i^{(x+1)} - \tilde{\mathbf{U}}_j^{(x+1)}) - \mathbf{g}_{ij}(\theta_i^{(x+1)} - \theta_j^{(x+1)})] \end{cases} \quad (10)$$

Formula (10) can be further simplified:

$$\begin{cases} \tilde{\mathbf{P}}_i^{\text{ls}(x)}\tilde{\mathbf{U}}_i^{(x-1)} \approx \tilde{\mathbf{P}}_i^{\text{ls}(x+1)}\tilde{\mathbf{U}}_i^{(x)} \\ \tilde{\mathbf{Q}}_i^{\text{ls}(x)}\tilde{\mathbf{U}}_i^{(x-1)} \approx \tilde{\mathbf{Q}}_i^{\text{ls}(x+1)}\tilde{\mathbf{U}}_i^{(x)} \end{cases} \quad (11)$$

The derivations of (10) and (11) are given in Supplementary Material C. Therefore, it is easy to arrange the modified equation for the node power injection based on the direct derivation.

$$\begin{cases} \tilde{\mathbf{P}}_i^{\text{ls}(x+1)} = \frac{\tilde{\mathbf{P}}_i^{\text{ls}(0)}}{\tilde{\mathbf{U}}_i^{(x)}} \\ \tilde{\mathbf{Q}}_i^{\text{ls}(x+1)} = \frac{\tilde{\mathbf{Q}}_i^{\text{ls}(0)}}{\tilde{\mathbf{U}}_i^{(x)}} \end{cases} \Rightarrow \begin{bmatrix} \tilde{\mathbf{P}}^{\text{ls}(x+1)} \\ \tilde{\mathbf{Q}}^{\text{ls}(x+1)} \end{bmatrix} = \boldsymbol{\Psi}_{\text{AC}}(\tilde{\mathbf{U}}^{(x)}) \quad (12)$$

where  $\boldsymbol{\Psi}_{\text{AC}}(\cdot)$  is the mathematical notation of the modified equation for node power injection in AC distribution network.

By associating (1) and (12), the vector form of the fixed-point iteration for AC node power injections can be formulated by:

$$\begin{bmatrix} \tilde{\mathbf{P}}^{\text{ls}(x+1)} \\ \tilde{\mathbf{Q}}^{\text{ls}(x+1)} \end{bmatrix} = \boldsymbol{\Psi}_{\text{AC}} \left( \boldsymbol{\Phi}_{\text{AC}}^{-1} \left( \begin{bmatrix} \tilde{\mathbf{P}}^{\text{ls}(x)} \\ \tilde{\mathbf{Q}}^{\text{ls}(x)} \end{bmatrix} \right) \right) = \boldsymbol{\Xi}_{\text{AC}} \left( \begin{bmatrix} \tilde{\mathbf{P}}^{\text{ls}(x)} \\ \tilde{\mathbf{Q}}^{\text{ls}(x)} \end{bmatrix} \right) \quad (13)$$

where  $\boldsymbol{\Xi}_{\text{AC}}(\cdot)$  is the mathematical notation for the fixed-point equations for AC distribution network with respect to node power injection.

A comparison of the fixed-point iteration process for different lossy power flow models is shown in Fig. 2. When  $x > 0$ , the existing model estimates the losses from  $[\tilde{\mathbf{U}}^{(x)}, \boldsymbol{\theta}^{(x)}]^T$  and regards them as an approximation for the next iteration, then modifies  $[\tilde{\mathbf{P}}^{(x+1)}, \tilde{\mathbf{Q}}^{(x+1)}]^T$  as a new operating point to calculate the  $(x+1)^{\text{th}}$  solution  $[\tilde{\mathbf{U}}^{(x+1)}, \boldsymbol{\theta}^{(x+1)}]^T$  by (1). In contrast, the proposed lossy power flow model presumes that  $[\tilde{\mathbf{U}}^{(x+1)}, \boldsymbol{\theta}^{(x+1)}]^T$  is known, which means that  $[\tilde{\mathbf{P}}\tilde{\mathbf{L}}^{(x+1)}, \tilde{\mathbf{Q}}\tilde{\mathbf{L}}^{(x+1)}]$  has been compensated implicitly in the power flow of the AC distribution network. Utilizing the characteristics of the distribution network, and through reasonable assumptions and derivations,  $[\tilde{\mathbf{P}}^{(x+1)}, \tilde{\mathbf{Q}}^{(x+1)}]^T$  can be modified directly using the recent known  $\tilde{\mathbf{U}}^{(x)}$ .

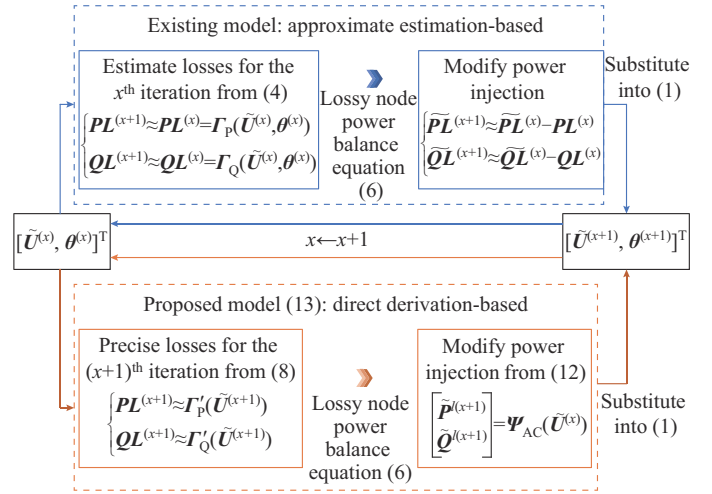


Fig. 2. A comparison of fixed-point iteration process for different lossy power flow models.

### C. Extension of Proposed Lossy Power Flow Model for DC Distribution Networks

The potential advantages of the lossy power flow model for the AC distribution network in Fig. 2 is also applicable to the DC case. Phase angle differences and reactive power injections are not considered in DC distribution networks. Accordingly, the DC branch losses allocated to nodes are special cases of (3) and (4):

$$\overline{P}\tilde{L}_{ij} = \overline{P}\tilde{L}_{ij}^i + \overline{P}\tilde{L}_{ij}^j = \bar{g}_{ij}(\bar{U}_i - \bar{U}_j)^2 \quad (14)$$

$$\overline{P}\tilde{L}_{ij}^i = \bar{g}_{ij}[(\bar{U}_i - 1)(\bar{U}_i - \bar{U}_j)] \quad (15)$$

Similarly, the lossy power balance equation for DC distribution network can be organized as a simplified version of (6):

$$\begin{aligned} \bar{P}_i &= \bar{P}_i^G - \bar{P}_i^D = \bar{P}_i^{\text{ls}(0)} + \sum_{j \in \kappa} \overline{P}\tilde{L}_{ij}^{i(0)} = \\ & \bar{P}_i^{\text{ls}(1)} + \sum_{j \in \kappa} \overline{P}\tilde{L}_{ij}^{i(1)} = \dots = \bar{P}_i^{\text{ls}(x)} + \sum_{j \in \kappa} \overline{P}\tilde{L}_{ij}^{i(x)} \end{aligned} \quad (16)$$

The linear approximation of the DC branch flows and the relationship with the DC node power injections are given by:

$$\bar{P}_i^{\text{ls}}(\bar{\mathbf{U}}) = \text{pol} \cdot \sum_{j \in \kappa} \bar{P}_{ij}^{\text{ls}}(\bar{\mathbf{U}}) \approx \text{pol} \cdot \sum_{j \in \kappa} \mathbf{g}_{ij}(\bar{U}_i - \bar{U}_j) \quad (17)$$

According to (17), the branch flows and losses for the  $x^{\text{th}}$  and the  $(x+1)^{\text{th}}$  iterations are:

$$\begin{cases} \bar{P}_{ij}^{\text{ls}(x)} = \bar{g}_{ij}(\bar{U}_i^{(x)} - \bar{U}_j^{(x)}) \\ \bar{P}_{ij}^{\text{ls}(x+1)} = \bar{g}_{ij}(\bar{U}_i^{(x+1)} - \bar{U}_j^{(x+1)}) \end{cases} \quad (18)$$

$$\begin{cases} \bar{P}L_{ij}^{i(x)} \approx \bar{g}_{ij}(\bar{U}_i^{(x-1)} - 1)(\bar{U}_i^{(x)} - \bar{U}_j^{(x)}) \\ \bar{P}L_{ij}^{i(x+1)} \approx \bar{g}_{ij}(\bar{U}_i^{(x)} - 1)(\bar{U}_i^{(x+1)} - \bar{U}_j^{(x+1)}) \end{cases} \quad (19)$$

Substituting (18) into (17) yields  $\bar{P}_i^{\text{ls}(x)}$  and  $\bar{P}_i^{\text{ls}(x+1)}$ , and substituting (19) into (16) leads to the following approximation:

$$\begin{aligned} \sum_{j \in \bar{\kappa}} \bar{g}_{ij} \bar{U}_i^{(x-1)} (\bar{U}_i^{(x)} - \bar{U}_j^{(x)}) &= \sum_{j \in \bar{\kappa}} \bar{g}_{ij} \bar{U}_i^{(x)} (\bar{U}_i^{(x+1)} - \bar{U}_j^{(x+1)}) \approx \\ &\bar{P}_i^{\text{ls}(x)} \bar{U}_i^{(x-1)} = \bar{P}_i^{\text{ls}(x+1)} \bar{U}_i^{(x)} \end{aligned} \quad (20)$$

As a result, the DC distribution network version of (11) can be organized.

$$\bar{P}_i^{\text{ls}(x+1)} = \frac{\bar{P}_i^{\text{ls}(0)}}{\bar{U}_i^{(x)}} \Rightarrow \bar{\mathbf{P}}^{\text{ls}(x+1)} = \boldsymbol{\Psi}_{\text{DC}}(\bar{\mathbf{U}}^{(x)}) \quad (21)$$

where  $\boldsymbol{\Psi}_{\text{DC}}(\cdot)$  is the mathematical notation of the modified equation for node power injection in a DC distribution network.

Given (2) and (21), the vector form of the fixed-point iteration for DC node power injections can be formulated by:

$$\bar{\mathbf{P}}^{\text{ls}(x+1)} = \boldsymbol{\Psi}_{\text{DC}}(\boldsymbol{\Phi}_{\text{DC}}^{-1}(\bar{\mathbf{P}}^{\text{ls}(x)})) = \boldsymbol{\Xi}_{\text{DC}}(\bar{\mathbf{P}}^{\text{ls}(x)}) \quad (22)$$

where  $\boldsymbol{\Xi}_{\text{DC}}(\cdot)$  is the mathematical notation of the fixed-point equations for DC distribution network with respect to node power injection.

Apparently, the fixed-point iteration problems formulated in (13) and (22) are mathematically equivalent. In other words, the direct derivation is applicable to both AC and DC distribution networks, which is fully compatible with the characteristics of DC distribution networks and has a natural advantage in terms of computational accuracy. Finally, the mismatches for the lossy power flows of AC and DC distribution networks can be unified by (13) and (22):

$$\begin{cases} \mathbf{F}_{\text{AC}} = [\Delta \bar{\mathbf{P}}^{\text{T}}, \Delta \bar{\mathbf{Q}}^{\text{T}}]^{\text{T}} \\ \mathbf{F}_{\text{DC}} = [\Delta \bar{\mathbf{P}}^{\text{T}}]^{\text{T}} \end{cases} \quad (23)$$

where  $\mathbf{F}_{\text{AC}}$  and  $\mathbf{F}_{\text{DC}}$  are the mismatch variable vectors of AC and DC distribution networks, respectively;  $\Delta \bar{\mathbf{P}}$  and  $\Delta \bar{\mathbf{Q}}$  are the mismatch variable vectors of active and reactive power injections at AC nodes, respectively; and  $\Delta \bar{\mathbf{P}}$  is the mismatch variable vector of active power injection at DC nodes.

### III. FULLY LOSSY POWER FLOW MODEL OF HYBRID AC-DC DISTRIBUTION NETWORKS

#### A. Lossy Power Flow Model for VSC

The VSC-based flexible equipment is a coupled component of the AC and DC distribution networks, which consists of four parts: transformers, phase reactors, AC filters, and rectifier (inverter) units, as shown in Fig. 3. The DC node connected to VSC converter is referred to as VSC-DC node, and the point of common coupling (PCC) node connected to the converter is referred to as the VSC-AC node. The power flow calculation of VSC station involves the power flow

equations of the VSC, the lossy power flow model of VSC, and the control modes.

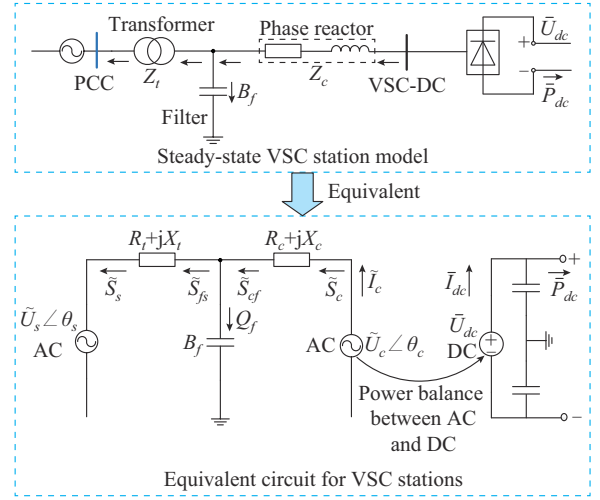


Fig. 3. VSC steady-state equivalent AC circuit.

The VSC power flow equations include the power balance equations at the PCC node on the AC side (24), the power balance equations of the VSC (25)-(28), and the active power balance equation between the AC side and the DC side (29).

$$\begin{cases} \tilde{P}_{s,l} = -g_{t,l} \tilde{U}_{s,l}^2 + \tilde{U}_{s,l} \tilde{U}_{f,l} (g_{t,l} \cos(\theta_{s,l} - \theta_{f,l}) + b_{t,l} \sin(\theta_{s,l} - \theta_{f,l})) \\ \tilde{Q}_{s,l} = b_{t,l} \tilde{U}_{s,l}^2 + \tilde{U}_{s,l} \tilde{U}_{f,l} (g_{t,l} \sin(\theta_{s,l} - \theta_{f,l}) - b_{t,l} \cos(\theta_{s,l} - \theta_{f,l})) \end{cases} \quad (24)$$

$$\begin{cases} \tilde{P}_{c,l} = g_{c,l} \tilde{U}_{c,l}^2 - \tilde{U}_{f,l} \tilde{U}_{c,l} (g_{c,l} \cos(\theta_{f,l} - \theta_{c,l}) - b_{c,l} \sin(\theta_{f,l} - \theta_{c,l})) \\ \tilde{Q}_{c,l} = -b_{c,l} \tilde{U}_{c,l}^2 + \tilde{U}_{f,l} \tilde{U}_{c,l} (g_{c,l} \sin(\theta_{f,l} - \theta_{c,l}) + b_{c,l} \cos(\theta_{f,l} - \theta_{c,l})) \end{cases} \quad (25)$$

$$\begin{cases} \tilde{P}_{f,l} = g_{t,l} \tilde{U}_{f,l}^2 - \tilde{U}_{f,l} \tilde{U}_{s,l} (g_{t,l} \cos(\theta_{s,l} - \theta_{f,l}) - b_{t,l} \sin(\theta_{s,l} - \theta_{f,l})) \\ \tilde{Q}_{f,l} = -b_{t,l} \tilde{U}_{f,l}^2 + \tilde{U}_{f,l} \tilde{U}_{s,l} (g_{t,l} \sin(\theta_{s,l} - \theta_{f,l}) + b_{t,l} \cos(\theta_{s,l} - \theta_{f,l})) \end{cases} \quad (26)$$

$$\begin{cases} \tilde{P}_{e,f,l} = -g_{c,l} \tilde{U}_{f,l}^2 + \tilde{U}_{f,l} \tilde{U}_{c,l} (g_{c,l} \cos(\theta_{f,l} - \theta_{c,l}) + b_{c,l} \sin(\theta_{f,l} - \theta_{c,l})) \\ \tilde{Q}_{e,f,l} = b_{c,l} \tilde{U}_{f,l}^2 + \tilde{U}_{f,l} \tilde{U}_{c,l} (g_{c,l} \sin(\theta_{f,l} - \theta_{c,l}) - b_{c,l} \cos(\theta_{f,l} - \theta_{c,l})) \end{cases} \quad (27)$$

$$\tilde{Q}_{f,l} = -b_{f,l} \tilde{U}_{f,l}^2 \quad (28)$$

$$\bar{P}_{dc,l} = -\tilde{P}_{c,l} - \tilde{P}L_{\text{vsc},l} \quad \forall l \in \ell \quad (29)$$

The VSC losses can be described as a quadratic polynomial with respect to the reactor current  $\tilde{I}_{c,l}$ :

$$\begin{aligned} \tilde{P}L_{\text{vsc},l} &= a + b \tilde{I}_{c,l} + c \tilde{I}_{c,l}^2 \\ \tilde{I}_{c,l} &= \frac{\sqrt{\tilde{P}_{c,l}^2 + \tilde{Q}_{c,l}^2}}{\sqrt{3} \tilde{U}_{c,l}} \end{aligned} \quad (30)$$

With fully controllable electronic devices such as insulated-gate bipolar transistors (IGBTs) and the vector control technique, the control scheme of a VSC station takes a two-loop cascaded structure: the  $d$ -axis control group and the  $q$ -axis control group. The modeling of each VSC requires these two

references. The  $d$ -axis control group is also called active power control group. It mainly consists of 3 categories: constant  $\bar{U}_{dc}$  control mode, constant  $\tilde{P}_s$  control mode, and voltage-power droop control mode ( $\bar{U}_{dc}$  droop). The  $q$ -axis control group contains two control modes, i.e., constant  $\tilde{Q}_s$  control mode and constant  $\tilde{U}_s$  control mode [12]. Consequently, a VSC station has six different control modes, as shown in Table I.

TABLE I  
MODELING OF A VSC: CONTROL MODES AND DEVICE TYPES

Grid-connected interface type	Control mode No.	Control mode		Device type	
		$d$ -axis control	$q$ -axis control	AC	DC
Grid-following	1	Constant $\tilde{P}_s$	Constant $\tilde{Q}_s$	$PQ$	I
	2	Constant $\tilde{P}_s$	Constant $\tilde{U}_s$	$PV$	
Grid-forming	3	Constant $\bar{U}_{dc}$	Constant $\tilde{Q}_s$	$PQ$	II
	4	Constant $\bar{U}_{dc}$	Constant $\tilde{U}_s$	$PV$	
Grid-forming or grid-following	5	$\bar{U}_{dc}$ droop	Constant $\tilde{Q}_s$	$PQ$	III
	6	$\bar{U}_{dc}$ droop	Constant $\tilde{U}_s$	$PV$	

On the AC side, converters can be deemed as  $PV$  or  $PQ$  devices based on their control modes and the demands of the distribution network. Control modes 1, 3, and 5 have the same  $q$ -axis reference, and the VSCs are regarded as  $PQ$  nodes. While control modes 2, 4, and 6 have the same  $q$ -axis reference, and the VSCs are regarded as  $PV$  nodes. In addition, for the power flow solvability, a DC distribution network with  $n_{dc}$  nodes should have at least one VSC selected as the DC slack node II (control modes 3 or 4) or node III (control modes 5 or 6), and no more than one node II. For example, a DC distribution network adopting DC slack node control has only one node II and  $(n_{dc} - 1)$  nodes I (control modes 1 or 2); and a DC distribution network adopting  $\bar{U}_{dc}$  droop control has  $m$  ( $m \geq 1$ ) nodes III and  $(n_{dc} - m)$  nodes I.

From the perspective of the VSC-AC node, the DC voltage can be controlled when a converter operates under DC voltage control (control modes 3-6), via either DC slack node control or droop control. For DC slack node control, the VSC is conceptualized as a grid-forming converter, whereas under  $\bar{U}_{dc}$  droop control, the VSC possesses the flexibility to function as either a grid-forming or a grid-following converter. Otherwise, the DC node should adopt the role of node I to regulate its own power, in which circumstance the VSC is characterized as a grid-following converter.

When a converter is under DC voltage control, either a slack node control (e.g., modes 3 and 4) or droop control (e.g., modes 5 and 6), the active power injection  $\tilde{P}_s$  in the AC distribution network is not known beforehand, since it depends on the active power needed on the DC side to control the DC voltage and the losses of the VSCs. Therefore, the power flow calculation involves an additional iteration step, i.e., DC slack node or droop node iteration [7], [10]. The initial active power injected into the AC distribution network needs to be estimated at the first step of calculation. For this purpose, two necessary assumptions are required.

1) The VSC is approximated as a lossless state.

2) For the DC slack bus, its power injection is estimated to be the negative summation of the active power injections from other nodes, while the estimation of power injection at PCC for DC droop nodes is assumed to be the negative value of power reference. The power reference is set according to the normal operating points. In contrast, when the converter is in other modes such as constant  $\tilde{P}_s$  control (corresponding to modes 1 and 2), the active power injection in the AC distribution network is kept constant without additional iteration steps.

$$\begin{cases} \tilde{P}_{s,d}^{(0)} = -\bar{P}_{dc,d}^{(0)} & \forall d \in \ell_{dp} \\ \tilde{P}_{s,m}^{(0)} = -\sum_{d \in \ell_{dp}} \tilde{P}_{s,d}^{(0)} - \sum_{l \in \ell_{sl}} \tilde{P}_{s,l} & \forall m \in \ell_{ma} \end{cases} \quad (31)$$

The initial estimations of AC power flow  $\tilde{I}_{c,l}$  and  $\tilde{U}_{c,l}$  can be solved by substituting  $\tilde{P}_{s,m}^{(0)}$  and the known control variables  $[\tilde{P}^{ls(0)}, \tilde{Q}^{ls(0)}]^T$  of nodes into (1) [7]:

$$\begin{cases} \tilde{I}_{c,l} = \frac{\tilde{P}_{s,l} - j\tilde{Q}_{s,l}}{\tilde{U}_{s,l}^*} \\ \tilde{U}_{c,l} = \tilde{U}_{s,l} - Z_{c,l} \frac{\tilde{P}_{s,l} - j\tilde{Q}_{s,l}}{\tilde{U}_{s,l}^*} \end{cases} \quad (32)$$

Given (25) and (32), the active power injection at the converter side can be reformulated as:

$$\tilde{P}_{c,l}^{(x)} = \boldsymbol{\theta}_C(\tilde{P}_{s,l}^{(x)}) \quad (33)$$

where  $\boldsymbol{\theta}_C(\cdot)$  is the mathematical notation for the linear equation obtained by uniting (25) and (32).

Furthermore,  $\bar{P}_{vsc,l}$  is calculated by (30) and substituted into (2) to solve the power flow of DC distribution network, and  $\tilde{P}_{c,l}$  can be updated after obtaining the DC node voltages using (29). However, the traditional active power injection calculation method based on Newton-Raphson (NR) iteration is highly nonlinear. To decrease the computational complexity, the assumptions in Supplementary Material A can be called back for linear approximation, and the reactive power injection at PCC node in (24) and the VSC active power injection in (25), (26)-(28) can be approximated as:

$$\begin{cases} \tilde{P}_{c,l} \approx \tilde{P}_{cf,l} \approx -g_{c,l}(\tilde{U}_{f,l} - \tilde{U}_{c,l}) + b_{c,l}(\theta_{f,l} - \theta_{c,l}) \\ \tilde{Q}_{s,l} \approx \tilde{Q}_{sf,l} \approx b_{l,l}(\tilde{U}_{s,l} - \tilde{U}_{f,l}) + g_{l,l}(\theta_{s,l} - \theta_{f,l}) \\ \tilde{P}_{sf,l} \approx -g_{l,l}(\tilde{U}_{s,l} - \tilde{U}_{f,l}) + b_{l,l}(\theta_{s,l} - \theta_{f,l}) \\ \tilde{Q}_{cf,l} \approx b_{c,l}(\tilde{U}_{f,l} - \tilde{U}_{c,l}) + g_{c,l}(\theta_{f,l} - \theta_{c,l}) \\ \tilde{Q}_{f,l} \approx -b_{f,l}\tilde{U}_{f,l} \end{cases} \quad (34)$$

Combining and rearranging items of (34) then yields:

$$\begin{cases} \tilde{P}_{c,l} \approx g_{c,l}(\tilde{U}_{c,l} - \tilde{U}_{f,l}) + b_{c,l}\theta_{fc,l} \\ \tilde{Q}_{s,l} \approx -b_{l,l}(\tilde{U}_{f,l} - \tilde{U}_{s,l}) + g_{l,l}\theta_{sf,l} \\ \Delta f_{P,l} = \tilde{P}_{cf,l} - \tilde{P}_{sf,l} \approx g_c\tilde{U}_c + g_{l,l}\tilde{U}_{s,l} - (g_{c,l} + g_{l,l})\tilde{U}_{f,l} + b_{c,l}\theta_{fc,l} - b_{l,l}\theta_{sf,l} \\ \Delta f_{Q,l} = \tilde{Q}_{cf,l} - \tilde{Q}_{sf,l} - \tilde{Q}_{f,l} \approx -b_{c,l}\tilde{U}_{c,l} - b_{l,l}\tilde{U}_{s,l} + (b_{c,l} + b_{f,l} + b_{l,l})\tilde{U}_{f,l} + g_{c,l}\theta_{fc,l} - g_{l,l}\theta_{sf,l} \end{cases} \quad (35)$$

Due to the small  $b_f$  of the filter, the variation of  $\tilde{U}_{f,l}$  during the calculation is much smaller than that of  $\tilde{U}_{c,l}$ . In other words, the interference of the voltage magnitude of the filter on the results is negligible. Thus,  $\tilde{U}_{f,l}$  can be represented by a constant term  $C_f$ . The matrix form of the rigorous LPF model for VSC can be rearranged as:

$$\begin{bmatrix} \tilde{P}_c + G_c \tilde{U}_f \\ \tilde{Q}_s + B_{yf} \tilde{U}_f \\ (G_c + G_{yf}) \tilde{U}_f \\ -(B_c + B_{yf} + B_{sf}) \tilde{U}_f \end{bmatrix} = \begin{bmatrix} G_c & \mathbf{0} & B_c & \mathbf{0} \\ \mathbf{0} & B_{yf} & \mathbf{0} & G_{yf} \\ G_c & G_{yf} & B_c & -B_{yf} \\ -B_c & -B_{yf} & G_c & -G_{yf} \end{bmatrix} \begin{bmatrix} \tilde{U}_c \\ \tilde{U}_s \\ \theta_{fc} \\ \theta_{sf} \end{bmatrix} \Rightarrow \begin{bmatrix} \tilde{P}_c \\ \tilde{Q}_s \\ \Delta f_p \\ \Delta f_Q \end{bmatrix} = \Phi_{\text{VSC}} \begin{bmatrix} \tilde{U}_c \\ \tilde{U}_s \\ \theta_{fc} \\ \theta_{sf} \end{bmatrix} + C_f \quad (36)$$

Given (24), (33), and (36), the fixed-point iteration model and mismatch equations for VSC lossy power flow can be formulated as:

$$\begin{cases} \tilde{P}_{s,m}^{(x+1)} = \Psi_s(\Phi_{\text{VSC}}^{-1}(\Theta_c(\tilde{P}_{s,m}^{(x)}))) = \Xi_s(\tilde{P}_{s,m}^{(x)}) \\ F_{\text{VSC}} = [\Delta \tilde{P}_{s,m}^T]^T \end{cases} \quad (37)$$

where  $\Psi_s(\cdot)$  is the active power equation of (24); and  $m \in \ell_{ma}$  represents the  $m^{\text{th}}$  master VSC.

### B. Overall Framework

The overall framework of the proposed lossy power flow model for hybrid AC-DC distribution networks is shown in Algorithm 1.

---

**Algorithm 1:** overall framework of proposed lossy power flow model for hybrid AC-DC distribution networks

---

**Input:** basic data of hybrid AC-DC distribution network

**Output:** voltage magnitudes, phase angles, and branch flows of hybrid AC-DC distribution networks

- 1: Initialize:  $\tilde{x}$ ,  $\bar{x}$ ,  $x \leftarrow 0$ ,  $It_{\max} = 10$ , and  $\delta = 10^{-8}$
  - 2: Set initial values  $\tilde{P}^{\text{ls}(0)}$ ,  $\tilde{Q}^{\text{ls}(0)}$ ,  $\tilde{P}^{\text{ls}(0)}$ , and  $\tilde{P}_{s,m}^{(0)}$  from (6), (16), and (31)
  - 3: **while**  $((x \leq It_{\max}) \& (\delta < \|F_{\text{VSC}}\|))$  **do**
  - 4:   **if**  $((\tilde{x} = 0) \& (\bar{x} = 0))$  **then**
  - 5:     Solve the lossless AC-LPF  $[\tilde{U}^{(0)}, \theta^{(0)}]^T$  from (1)
  - 6:     Calculate  $\tilde{P}_{\text{VSC}}^{(0)}$  from (30)
  - 7:     Solve the lossless DC-LPF  $\tilde{U}^{(0)}$  from (2)
  - 8:   **else**
  - 9:     **for**  $\tilde{x} = 1, 2, \dots, It_{\max}$  **do**
  - 10:       Solve AC lossy power flow  $[\tilde{U}^{(\tilde{x})}, \theta^{(\tilde{x})}]^T$  from (13)
  - 11:       **if**  $\delta < \|F_{\text{AC}}\|$  **then**
  - 12:          $\tilde{x} \leftarrow \tilde{x} + 1$
  - 13:       **end if**
  - 14:     **end for**
  - 15:     Update VSC losses  $\tilde{P}_{\text{VSC}}^{(\tilde{x})}$  from (30)
  - 16:     **for**  $\bar{x} = 1, 2, \dots, It_{\max}$  **do**
  - 17:       Solve DC lossy power flow  $\tilde{U}^{(\bar{x})}$  from (22)
  - 18:       **if**  $\delta < \|F_{\text{DC}}\|$  **then**
  - 19:          $\bar{x} \leftarrow \bar{x} + 1$
  - 20:       **end if**
  - 21:     **end for**
  - 22:     Update fixed point of VSC  $\tilde{P}_{s,m}^{(\tilde{x})}$  from (37)
  - 23:   **end if**
  - 24:    $x \leftarrow x + 1$
  - 25: **end while**
- 

The framework is implemented using the asynchronous it-

eration method, i.e., the AC and DC distribution networks, and VSCs can be iterated sequentially. For small-scale hybrid AC-DC distribution networks, the convergence performance of the synchronous iteration method is better than that of the asynchronous one. However, in the case of multi-area interconnection, the number of nodes can be large, and the Jacobi matrix of the synchronous iteration method becomes complex. Thus, the implementation of the sparse technique for modifying the Jacobi matrix becomes more difficult, which increases the computation time. In contrast, the order of the Jacobi matrix of the asynchronous iteration method varies less with the distribution network scale, and the computational complexity does not increase significantly. In addition, the asynchronous iteration method simply extends the power flow calculation module for DC distribution networks on the original AC power flow calculation program, and then iterates between AC and DC distribution networks. Therefore, the asynchronous iteration method is easier to be implemented than the synchronous iteration method.

## IV. NUMERICAL RESULTS

Algorithm 1 was implemented in the MATLAB source toolbox MATPOWER [41]. Three hybrid AC-DC distribution networks, i.e., the modified IEEE 33 test feeders, the modified IEEE 33&69 test feeders, and the modified IEEE 123 test feeders, are obtained by modifying standard test systems, i.e., IEEE 33 test feeders, US PG&E 69 test feeders, and IEEE 123 test feeders, respectively. All programs required for the experiments are compiled in MATLAB 2020b, and all simulations are done on a personal computer with AMD4800H 3.20 GHz CPU and 16 GB of RAM. Detail information of all test cases can be found in Supplementary Material A.

### A. Lossy Power Flow Results for Sub-networks

The hybrid AC-DC distribution network contains AC sub-networks and DC sub-networks. To verify the superiority of the proposed lossy power model in terms of computational accuracy in AC and DC sub-networks, the experimental process needs to follow the principle of control variates. In other words, the same model must be used on the DC side (AC side) when analyzing the error on the AC side (DC side). We present the lossless LPF model in [16] as a comparison and extend it naturally to DC networks. The lossy model in [30] is denoted by the existing lossy power flow (E-lossy) model, and the model adopted in this paper is denoted by the proposed lossy power flow (P-lossy) model.

For ease of presentation, different hybrid models (HMs) are used to represent the sets of models for both AC and DC sub-networks.

- 1) HM1: lossless model in AC and DC sub-networks.
- 2) HM2: E-lossy model in AC and DC sub-networks.
- 3) HM3: E-lossy model in AC sub-network, and P-lossy model in DC sub-network.
- 4) HM4: P-lossy model in AC sub-network, and E-lossy model in DC sub-network.
- 5) HM5: P-lossy model in AC and DC sub-networks.

The root-mean-square error  $\varepsilon^{\text{RMSE}}$  and the maximum error  $\varepsilon^{\text{max}}$  (infinity norm) for all variables are calculated as:

$$\left\{ \begin{array}{l} \varepsilon_x^{RMSE} = \sqrt{\frac{1}{N} \sum_{i=1}^N (Y_i - f(x_i))^2} \\ \varepsilon_x^{\max} = \|Y_i - f(x_i)\|_{\infty} \\ x \in \{\tilde{U}_{AC}, \theta_{AC}, \tilde{P}_{AC}, \tilde{Q}_{AC}, \bar{U}_{DC}, \bar{P}_{DC}, \\ \tilde{U}_{VSC}, \theta_{VSC}, \tilde{P}_{VSC}, \tilde{Q}_{VSC}, \tilde{P}_{VSC}^{\tilde{L}}\} \end{array} \right. \quad (38)$$

The errors in (38) are computed for all the sub-network variables using all the steps in Algorithm 1, and the statistics are shown in Table II, including the errors of AC and DC node voltage magnitudes  $\tilde{U}_{AC}$  and  $\bar{U}_{DC}$ , the node voltage phase angles  $\theta_{AC}$ , the AC and DC active branch flows  $\tilde{P}_{AC}$  and  $\bar{P}_{DC}$ , and reactive branch flows  $\tilde{Q}_{AC}$ . Clearly, HM1 in Table II has the worst performance as it ignores the network losses. Moreover, by comparing HM2 and HM3 for DC sub-networks, the errors of the node voltage magnitude and branch flow of the P-lossy model are significantly smaller than those of the E-lossy model. Congruently, the same result can be observed by comparing HM4 and HM5. For AC sub-networks, the errors of node voltage magnitude and

branch flow of the P-lossy model are smaller than those of the E-lossy model. As can be observed from HM2 and HM4, the same can be found by comparing HM3 and HM5. In conclusion, the P-lossy model is proved to be advantageous compared with the existing models, both for AC and DC sub-networks. Furthermore, comparing HM1, HM2, and HM5, the errors of node voltage magnitudes and branch flows of the P-lossy model are smaller than other models, which indicates the superiority of the P-lossy model in solving the global power flows. Besides, some other attractive facts are found. Even if the same model is employed in the DC sub-network, there are still slight differences in the DC node voltage magnitudes and branch flow errors, which suggests that different AC lossy models can also affect the DC power flow results. In the modified IEEE 33&69 test feeders, for example, the P-lossy model is employed in both HM3 and HM5 for the AC sub-network, but the errors of  $\bar{U}_{DC}$  and  $\bar{P}_{DC}$  are different, as shown in Table II. Therefore, it is reasonable to infer that there are coupling effects between the models, and in particular, the AC lossy model has an impact on the DC power flow.

TABLE II  
ERROR STATISTICS OF DIFFERENT MODELS FOR ALL TEST CASES

Case name	HM	$\varepsilon^{RMSE}$						$\varepsilon^{\max}$					
		$\tilde{U}_{AC}$	$\theta_{AC}$	$\tilde{P}_{AC}$	$\tilde{Q}_{AC}$	$\bar{U}_{DC}$	$\bar{P}_{DC}$	$\tilde{U}_{AC}$	$\theta_{AC}$	$\tilde{P}_{AC}$	$\tilde{Q}_{AC}$	$\bar{U}_{DC}$	$\bar{P}_{DC}$
Modified IEEE 33 test feeders	HM1	$2.74 \times 10^{-3}$	$1.39 \times 10^{-1}$	$9.43 \times 10^{-2}$	$1.29 \times 10^{-1}$	$1.79 \times 10^{-4}$	$4.91 \times 10^{-3}$	$3.83 \times 10^{-3}$	$2.08 \times 10^{-1}$	$3.77 \times 10^{-1}$	$5.23 \times 10^{-1}$	$2.67 \times 10^{-4}$	$6.17 \times 10^{-3}$
	HM2	$2.27 \times 10^{-3}$	$1.05 \times 10^{-1}$	$6.44 \times 10^{-2}$	$9.54 \times 10^{-2}$	$6.31 \times 10^{-6}$	$1.95 \times 10^{-4}$	$4.47 \times 10^{-3}$	$1.71 \times 10^{-1}$	$2.40 \times 10^{-1}$	$3.67 \times 10^{-1}$	$8.28 \times 10^{-6}$	$3.62 \times 10^{-4}$
	HM3	$2.27 \times 10^{-3}$	$1.05 \times 10^{-1}$	$6.44 \times 10^{-2}$	$9.54 \times 10^{-2}$	$1.86 \times 10^{-11}$	$5.05 \times 10^{-10}$	$4.47 \times 10^{-3}$	$1.71 \times 10^{-1}$	$2.40 \times 10^{-1}$	$3.67 \times 10^{-1}$	$2.77 \times 10^{-11}$	$6.38 \times 10^{-10}$
	HM4	$1.95 \times 10^{-4}$	$6.67 \times 10^{-2}$	$4.77 \times 10^{-2}$	$5.90 \times 10^{-2}$	$6.31 \times 10^{-6}$	$1.95 \times 10^{-4}$	$3.75 \times 10^{-4}$	$9.63 \times 10^{-2}$	$2.17 \times 10^{-1}$	$2.64 \times 10^{-1}$	$8.28 \times 10^{-6}$	$3.62 \times 10^{-4}$
	HM5	$1.95 \times 10^{-4}$	$6.67 \times 10^{-2}$	$4.77 \times 10^{-2}$	$5.90 \times 10^{-2}$	$1.86 \times 10^{-11}$	$5.05 \times 10^{-10}$	$3.75 \times 10^{-4}$	$9.63 \times 10^{-2}$	$2.17 \times 10^{-1}$	$2.64 \times 10^{-1}$	$2.77 \times 10^{-11}$	$6.38 \times 10^{-10}$
Modified IEEE 33&69 test feeders	HM1	$5.72 \times 10^{-3}$	$3.36 \times 10^{-2}$	$1.08 \times 10^{-1}$	$6.08 \times 10^{-2}$	$3.11 \times 10^{-4}$	$5.94 \times 10^{-3}$	$1.37 \times 10^{-2}$	$7.88 \times 10^{-2}$	$3.26 \times 10^{-1}$	$1.76 \times 10^{-1}$	$7.16 \times 10^{-4}$	$9.79 \times 10^{-3}$
	HM2	$4.64 \times 10^{-3}$	$3.48 \times 10^{-2}$	$8.56 \times 10^{-2}$	$5.04 \times 10^{-2}$	$4.27 \times 10^{-4}$	$7.62 \times 10^{-3}$	$1.17 \times 10^{-2}$	$8.35 \times 10^{-2}$	$2.25 \times 10^{-1}$	$1.24 \times 10^{-1}$	$9.25 \times 10^{-4}$	$1.07 \times 10^{-7}$
	HM3	$4.64 \times 10^{-3}$	$3.48 \times 10^{-2}$	$8.56 \times 10^{-2}$	$5.04 \times 10^{-2}$	$9.94 \times 10^{-6}$	$1.79 \times 10^{-4}$	$1.17 \times 10^{-2}$	$8.35 \times 10^{-2}$	$2.25 \times 10^{-1}$	$1.24 \times 10^{-1}$	$2.18 \times 10^{-5}$	$2.47 \times 10^{-4}$
	HM4	$2.45 \times 10^{-4}$	$1.08 \times 10^{-2}$	$7.57 \times 10^{-3}$	$9.61 \times 10^{-3}$	$4.17 \times 10^{-4}$	$7.43 \times 10^{-3}$	$8.66 \times 10^{-4}$	$3.43 \times 10^{-2}$	$5.04 \times 10^{-2}$	$3.47 \times 10^{-2}$	$9.02 \times 10^{-4}$	$1.04 \times 10^{-2}$
	HM5	$2.45 \times 10^{-4}$	$1.08 \times 10^{-2}$	$7.57 \times 10^{-3}$	$9.61 \times 10^{-3}$	$2.29 \times 10^{-7}$	$4.13 \times 10^{-6}$	$8.66 \times 10^{-4}$	$3.43 \times 10^{-2}$	$5.04 \times 10^{-2}$	$3.47 \times 10^{-2}$	$4.99 \times 10^{-7}$	$5.64 \times 10^{-6}$
Modified IEEE 123 test feeders	HM1	$1.86 \times 10^{-5}$	$1.76 \times 10^{-4}$	$1.68 \times 10^{-3}$	$1.20 \times 10^{-3}$	$1.45 \times 10^{-3}$	$1.40 \times 10^{-2}$	$4.25 \times 10^{-5}$	$3.08 \times 10^{-4}$	$5.46 \times 10^{-3}$	$5.20 \times 10^{-3}$	$3.16 \times 10^{-3}$	$2.26 \times 10^{-2}$
	HM2	$1.70 \times 10^{-5}$	$1.74 \times 10^{-4}$	$1.50 \times 10^{-3}$	$6.76 \times 10^{-4}$	$1.13 \times 10^{-4}$	$1.37 \times 10^{-3}$	$4.00 \times 10^{-5}$	$3.06 \times 10^{-4}$	$5.14 \times 10^{-3}$	$2.49 \times 10^{-3}$	$2.38 \times 10^{-4}$	$2.63 \times 10^{-3}$
	HM3	$1.70 \times 10^{-5}$	$1.74 \times 10^{-4}$	$1.50 \times 10^{-3}$	$6.76 \times 10^{-4}$	$1.69 \times 10^{-9}$	$4.81 \times 10^{-8}$	$4.00 \times 10^{-5}$	$3.06 \times 10^{-4}$	$5.14 \times 10^{-3}$	$2.49 \times 10^{-3}$	$7.56 \times 10^{-9}$	$1.23 \times 10^{-7}$
	HM4	$1.46 \times 10^{-5}$	$2.29 \times 10^{-5}$	$4.49 \times 10^{-4}$	$5.38 \times 10^{-4}$	$1.13 \times 10^{-4}$	$1.37 \times 10^{-3}$	$3.56 \times 10^{-5}$	$5.37 \times 10^{-5}$	$1.66 \times 10^{-3}$	$2.80 \times 10^{-3}$	$2.38 \times 10^{-4}$	$2.63 \times 10^{-3}$
	HM5	$1.46 \times 10^{-5}$	$2.29 \times 10^{-5}$	$4.49 \times 10^{-4}$	$5.38 \times 10^{-4}$	$1.04 \times 10^{-9}$	$2.96 \times 10^{-8}$	$3.56 \times 10^{-5}$	$5.37 \times 10^{-5}$	$1.66 \times 10^{-3}$	$2.80 \times 10^{-3}$	$4.65 \times 10^{-9}$	$7.57 \times 10^{-8}$

### B. Lossy Power Flow Results for VSCs

Two test cases, the modified IEEE 33&69 and modified IEEE 123 test feeders, are used to verify the effectiveness of the P-lossy model for MT-VSCs.

For the modified IEEE 33&69 test feeders, VSCs 2, 4, and 7 are under DC voltage control corresponding to control mode 3, while the other VSCs employ mode 2 to control their own active power, and act as the *PV* devices. In the modified IEEE 123 test feeders, a hybrid control mode is implemented, with VSCs 1, 4, and 6 as DC slack nodes, i.e., control mode 4. VSCs 3 and 7 regulate the voltage with *U-P* droop control, i.e., control mode 5; and VSCs 2, 5, and 8 utilize control mode 1 and act as the *PQ* devices.

Different lossy power flow models for VSC are shown in

Table III. In [34], the lossless DCPF model and the E-lossy model are implemented for the AC and DC distribution networks, respectively, and the benchmark NR method is used to calculate the VSC power flow. Another model, VSC-NLPPF, is consistent with [34] in solving the VSC power flow, while the P-lossy model is used to solve the AC and DC power flows. Finally, the benchmark power flow for the whole system is solved by the NR method.

Since the DCPF is employed in [34], only VSC voltage phase angles  $\theta_c$  and active power injected into VSCs  $\tilde{P}_c$  are compared. Here, we do not use (38) to measure the VSC power flow errors since  $\varepsilon^{RMSE}$  and  $\varepsilon^{\max}$  only evaluate the average and maximum errors. To identify the power flow errors of each VSC, the relative error  $\varepsilon^{RE}$  is defined as:

TABLE III  
DIFFERENT LOSSY POWER FLOW MODELS FOR VSCs IN HYBRID AC-DC  
DISTRIBUTION NETWORKS

Type	[34]	VSC-NLPF	Proposed
AC distribution network	Lossless DCPF	P-lossy	P-lossy
DC distribution network	E-lossy	P-lossy	P-lossy
MT-VSC	NR	NR	P-lossy

$$\varepsilon_x^{RE} = \frac{Y_i - f(x_i)}{Y_i} \quad x \in \{\theta_c, |\tilde{P}_c|\} \quad (39)$$

The VSC power flow errors for different network scales and control modes are shown in Fig. 4. The left y-axes of subfigures represent  $\varepsilon_{\theta_c}^{RE}$  and  $\varepsilon_{|\tilde{P}_c|}^{RE}$ , which are marked by different colored bars. While the right y-axes of subfigures represent the values of variables  $\theta_c$  and  $|\tilde{P}_c|$ , which marked by different shapes of scatters.

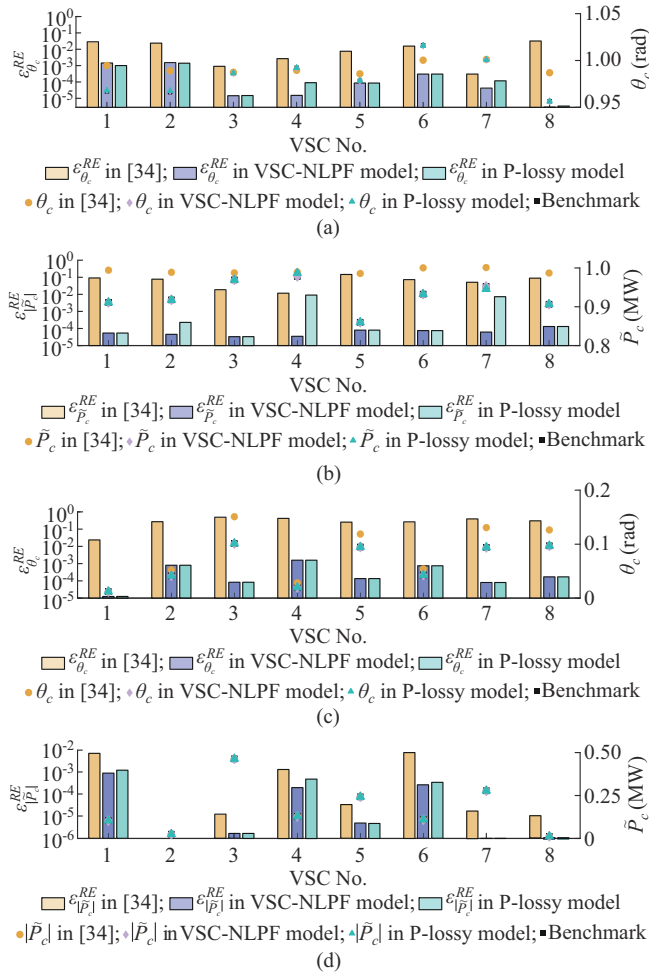


Fig. 4. VSC power flow errors for different network scales and control modes. (a) Phase angle in modified IEEE 33&69 test feeders. (b) Power injection in modified IEEE 33&69 test feeders. (c) Phase angle in modified IEEE 123 test feeders. (d) Power injection in modified IEEE 123 test feeders.

In Fig. 4, the voltage phase angles of the P-lossy model are highly consistent with the NLPF, while the errors calculated by the model in [34] is significantly larger than those

of the P-lossy model. In addition, the errors of the P-lossy model for VSC active power injection are also smaller than those of model in [34]. Obviously, the inaccurate DCPF is employed in the AC distribution network in [34], enlarging the power flow error injected into the VSC from the PCC. Consequently, although the model in [34] preserves the non-linearity of the VSC, it does not guarantee satisfactory results. Compared with NLPF, the performance of the P-lossy model for VSC power injections is not as stable as the voltage phase angles, especially for the grid-forming VSCs, as shown in Fig. 4(b). Nevertheless, in a global view, the P-lossy model still has a significant advantage over the model in [34], regardless of whether the VSC is a *PQ* or *PV* device, or whether it is a grid-forming or grid-following VSC.

In summary, at the system level, the P-lossy model shows excellent accuracy performance, no matter it is applied in AC, DC, or hybrid distribution networks. At the device level, the same is true for the P-lossy model.

### C. Convergence Analysis

In addition to comparing the solution accuracies of different models, it is also significant to verify the advantages of the P-lossy model in terms of convergence performance. The difference in computational time arises from two main aspects, i.e., the external iteration process and the internal iteration process.

The purpose of the external iteration is to make the active power of the slack VSC at the PCC node close to the true value, which represents the number of iterations for the whole hybrid AC-DC distribution network, whereas the internal iteration is used to solve the fixed-point problem for both AC and DC sub-networks. The external iterations and computational time of different models are shown in Table IV, including the number of external iterations and the computational time for 100 simulations. HM4 and HM5 are computationally efficient, with the computational time reduced by 6.43% and 20.22%, respectively, which is attributed to the excellent performance of the P-lossy model. In addition, HM5 ranks first in all test cases, while the rest of the hybrid models have slightly different rankings.

TABLE IV  
NUMBER OF EXTERNAL ITERATIONS AND COMPUTATIONAL TIME

Case name	HM	Number of external iterations	Computational time (ms)
Modified IEEE 33 test feeders	HM2	5	2632
	HM3	5	2487
	HM4	5	2073
	HM5	5	2010
	HM2	5	5055
Modified IEEE 33&69 test feeders	HM3	5	5057
	HM4	5	4217
	HM5	5	4162
	HM2	5	5330
	Modified IEEE 123 test feeders	HM3	5
HM4		6	4967
HM5		6	4831

The modified IEEE 33 test case is implemented for the analysis of the internal iterations. HM3 and HM5 are used to compare the convergence performance of the AC sub-network, and the results are shown in Fig. 5(a). And HM4 and HM5 are used to compare the convergence performance of the DC subnetwork, and the results are shown in Fig. 5(b).

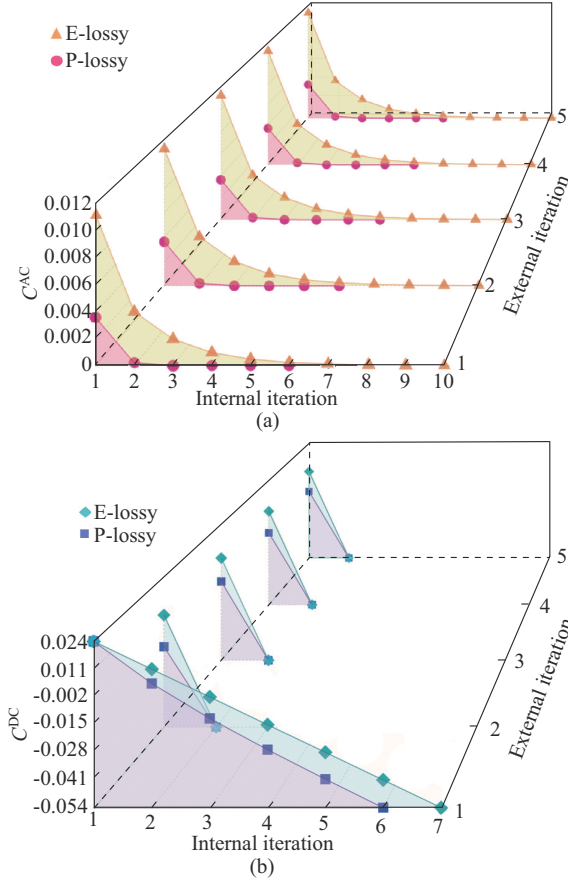


Fig. 5. AC and DC convergences of different lossy power flow models. (a) AC sub-network. (b) DC sub-network.

The P-lossy model converges at the 6<sup>th</sup> iteration, while the model in [30] still does not converge at the 10<sup>th</sup> iteration. In fact, it converges at the 23<sup>rd</sup> iteration. Similarly, the smaller area enclosed by the curves and axes of the P-lossy model means that it converges faster, requiring at most 6 iterations to converge, while the E-lossy model requires 7 iterations. By comparison, the P-lossy model not only improves the convergence performance of AC and DC sub-networks, but also effectively reduces the computational time.

#### D. Robustness Analysis of Overall Networks

The actual operating state of the distribution network is stochastic in nature, and there is a need to discuss whether the P-lossy model can maintain its expected functionality and performance in the face of uncertainties or perturbations. For this reason, Latin hypercube sampling is used for stochastically generating 1000 scenarios within a predefined range. Different ranges of variables are selected based on the characteristics of variables, e.g., the AC and DC load consumptions are calculated based on the preset demand con-

sumptions multiplied by a coefficient drawn stochastically in a stratified manner from a uniform distribution over the interval [0.5, 2]. The distributed renewable energy generation is calculated from the interval [0.3, 0.6]. The box and scatter plots of  $\epsilon^{RMSE}$  for different models under stochastic generation and demand are shown in Fig. 6.

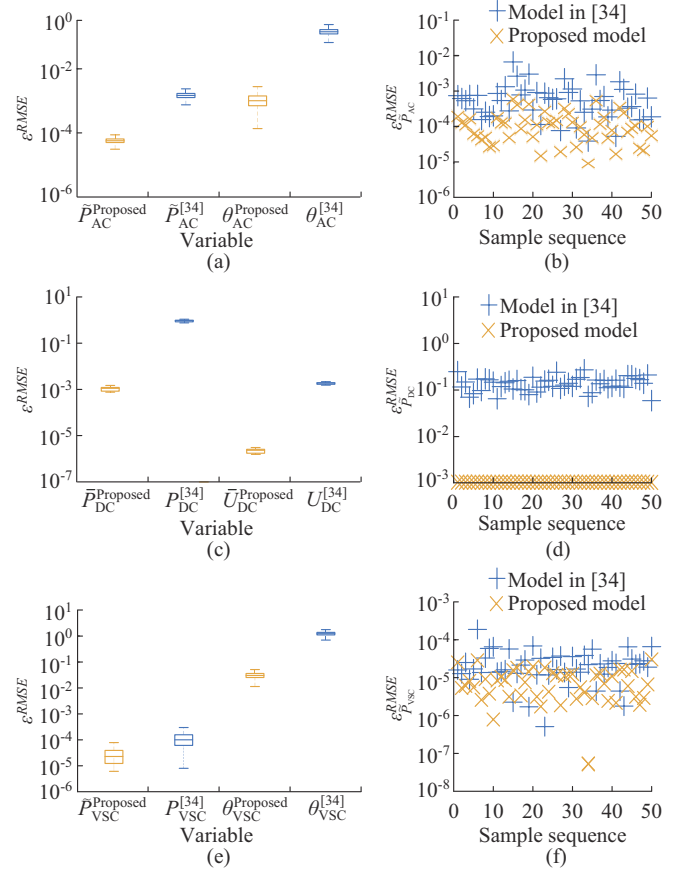


Fig. 6. Box and scatter plots of  $\epsilon^{RMSE}$  for different models. (a) Box plot for AC sub-network. (b) Scatter plot for AC sub-network. (c) Box plot for DC sub-network. (d) Scatter plot for DC sub-network. (e) Box plot for MT-VSC. (f) Scatter plot for MT-VSC.

In Fig. 6, the power flow errors for AC and DC sub-networks and VSC are shown from left to right. For the AC network, the errors of the P-lossy model are always less than those of the model in [34]. To compare more clearly the performance of the two models for AC power flows, Fig. 6 records the errors for different stochastic samples. Obviously, the errors of the P-lossy model are smaller and more centrally distributed, which implies stronger robustness. For the DC sub-network, the power flow errors of the P-lossy model are all significantly smaller than those of the model in [34].

For the VSC, although the nonlinearity is preserved in [34], the errors of both the node voltage magnitude and power injection are larger than those of the P-lossy model, which further demonstrates the good robustness of the P-lossy model in stochastic scenarios.

Since DCPF does not consider voltage magnitude or reactive power, the model in [34] is computationally efficient and maintains a good performance in solving active branch

flows and voltage phase angles. However, ignoring the effects of voltage magnitude and reactive power makes this model unable to accurately calculate the power flow of the VSC, and the penetration of distributed energy sources increases the risk of errors. Meanwhile, although voltage magnitude and reactive power are considered in HM2, this model is only applicable to transmission networks and performs poorly in hybrid AC-DC distribution networks. In contrast, the P-lossy model highly matches the characteristics of the distribution network.

To check the performance of the P-lossy model comprehensively, we employ the modified IEEE 33 test case and the modified IEEE 123 test case, and compare the average errors  $\hat{\epsilon}^{RMSE}$  and  $\hat{\epsilon}^{\max}$  for all variables, as shown in Tables V and VI, respectively. All test results illustrate that the P-lossy model has almost an order of magnitude advantage in terms of computational accuracy, and whether in AC sub-networks, DC sub-networks, or VSCs, its applicability and robustness under uncertainty generation and demand scenarios are further demonstrated.

TABLE V  
RMSES FOR DIFFERENT MODELS UNDER STOCHASTIC GENERATION AND DEMAND

Case name	Model	RMSE										
		$\tilde{U}_{AC}$	$\theta_{AC}$	$\tilde{P}_{AC}$	$\tilde{Q}_{AC}$	$\tilde{U}_{DC}$	$\tilde{P}_{DC}$	$\tilde{U}_{VSC}$	$\theta_{VSC}$	$\tilde{P}_{VSC}$	$\tilde{Q}_{VSC}$	$\tilde{PL}_{VSC}$
Modified IEEE 33 test feeders	P-lossy [34]	$2.97 \times 10^{-4}$	$1.12 \times 10^{-1}$	$8.11 \times 10^{-2}$	$9.89 \times 10^{-2}$	$2.05 \times 10^{-11}$	$5.56 \times 10^{-10}$	$3.54 \times 10^{-4}$	$1.19 \times 10^{-1}$	$2.84 \times 10^{-4}$	1.98	$9.39 \times 10^{-2}$
	HM2	$3.92 \times 10^{-3}$	$1.88 \times 10^{-1}$	$1.14 \times 10^{-1}$	$1.65 \times 10^{-1}$	$1.20 \times 10^{-5}$	$3.75 \times 10^{-4}$	$3.57 \times 10^{-3}$	$1.98 \times 10^{-1}$	$8.87 \times 10^{-4}$	2.02	$9.48 \times 10^{-2}$
Modified IEEE 123 test feeders	P-lossy [34]	$1.42 \times 10^{-5}$	$3.67 \times 10^{-5}$	$7.21 \times 10^{-4}$	$8.63 \times 10^{-4}$	$6.41 \times 10^{-10}$	$6.70 \times 10^{-10}$	$1.48 \times 10^{-5}$	$1.27 \times 10^{-3}$	$6.50 \times 10^{-3}$	1.30	$7.22 \times 10^{-2}$
	HM2	$1.82 \times 10^{-5}$	$2.79 \times 10^{-4}$	$2.40 \times 10^{-3}$	$1.09 \times 10^{-3}$	$6.49 \times 10^{-5}$	$1.18 \times 10^{-3}$	$1.81 \times 10^{-5}$	$2.97 \times 10^{-2}$	$6.57 \times 10^{-3}$	1.31	$7.30 \times 10^{-2}$

TABLE VI  
 $\hat{\epsilon}^{\max}$  FOR DIFFERENT MODELS UNDER STOCHASTIC GENERATION AND DEMAND

Case name	Model	$\hat{\epsilon}^{\max}$										
		$\tilde{U}_{AC}$	$\theta_{AC}$	$\tilde{P}_{AC}$	$\tilde{Q}_{AC}$	$\tilde{U}_{DC}$	$\tilde{P}_{DC}$	$\tilde{U}_{VSC}$	$\theta_{VSC}$	$\tilde{P}_{VSC}$	$\tilde{Q}_{VSC}$	$\tilde{PL}_{VSC}$
Modified IEEE 33 test feeders	P-lossy [34]	$5.53 \times 10^{-4}$	$1.61 \times 10^{-1}$	$3.82 \times 10^{-1}$	$4.43 \times 10^{-1}$	$3.05 \times 10^{-11}$	$7.02 \times 10^{-10}$	$5.49 \times 10^{-4}$	$1.68 \times 10^{-1}$	$1.18 \times 10^{-3}$	3.41	$9.44 \times 10^{-2}$
	HM2	$6.57 \times 10^{-3}$	$2.96 \times 10^{-1}$	$4.06 \times 10^{-1}$	$6.35 \times 10^{-1}$	$1.58 \times 10^{-5}$	$6.96 \times 10^{-4}$	$6.18 \times 10^{-3}$	$2.95 \times 10^{-1}$	$6.04 \times 10^{-3}$	3.47	$1.64 \times 10^{-1}$
Modified IEEE 123 test feeders	P-lossy [34]	$4.27 \times 10^{-5}$	$8.27 \times 10^{-5}$	$2.56 \times 10^{-3}$	$4.42 \times 10^{-3}$	$5.35 \times 10^{-9}$	$8.69 \times 10^{-8}$	$4.27 \times 10^{-5}$	$3.53 \times 10^{-3}$	$1.59 \times 10^{-2}$	3.41	$7.07 \times 10^{-2}$
	HM2	$4.90 \times 10^{-5}$	$4.73 \times 10^{-4}$	$7.81 \times 10^{-3}$	$3.82 \times 10^{-3}$	$3.51 \times 10^{-4}$	$3.99 \times 10^{-3}$	$4.90 \times 10^{-5}$	$3.90 \times 10^{-3}$	$1.59 \times 10^{-2}$	3.44	$1.82 \times 10^{-1}$

In addition, the  $r/x$  ratios are adjusted in increments of 0.1 within the range of [0.1, 5] to compare the performance of different models in AC sub-networks. The conductors of the

DC sub-network are consistent with normal operating conditions. The variation of errors in the modified IEEE 123 test case is shown in Fig. 7.

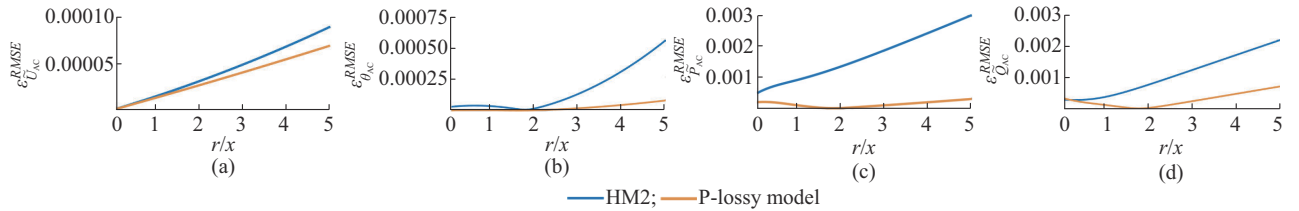


Fig. 7. Variation of errors with  $r/x$  ratios for different models in modified IEEE 123 test feeders. (a)  $\tilde{U}_{AC}$ . (b)  $\theta_{AC}$ . (c)  $\tilde{P}_{AC}$ . (d)  $\tilde{Q}_{AC}$ .

It can be observed that within the predefined range, the errors of the P-lossy model consistently remain at a lower level. The errors of HM2 exhibits a significant positive correlation with the  $r/x$  ratios, while the errors of the P-lossy model present a negative correlation when the  $r/x$  ratios are within (0, 1.8]. Such results indicate that the P-lossy model is particularly applicable to distribution networks with low  $r/x$  ratios.

To comprehensively verify the performance of the P-lossy model in hybrid networks, 1000 scenarios are also simulated from the interval [0.5, 5] to evaluate the robustness of sto-

chastic  $r/x$  ratios of AC sub-networks and resistance of DC sub-networks on the robustness of the P-lossy model. The average errors are computed for different network scales, as shown in Tables VII and VIII. The statistical results show that the average errors for AC or DC sub-networks of the P-lossy model are significantly lower than those of the existing models under stochastic  $r/x$  ratios or DC resistance. In conclusion, the P-lossy model maintains superior performance under various stochastic perturbations.

TABLE VII  
RMSEs FOR DIFFERENT MODELS UNDER STOCHASTIC LINE CONDUCTORS IN AC AND DC SUB-NETWORKS

Case name	Model	RMSE										
		$\tilde{U}_{AC}$	$\theta_{AC}$	$\tilde{P}_{AC}$	$\tilde{Q}_{AC}$	$\tilde{U}_{DC}$	$\tilde{P}_{DC}$	$\tilde{U}_{VSC}$	$\theta_{VSC}$	$\tilde{P}_{VSC}$	$\tilde{Q}_{VSC}$	$\tilde{PL}_{VSC}$
Modified IEEE 33 test feeders	P-lossy [34]	$4.79 \times 10^{-4}$	$2.08 \times 10^{-5}$	$1.22 \times 10^{-1}$	$1.75 \times 10^{-1}$	$3.15 \times 10^{-11}$	$7.22 \times 10^{-10}$	$5.48 \times 10^{-4}$	$2.17 \times 10^{-1}$	$1.27 \times 10^{-3}$	2.14	$9.89 \times 10^{-2}$
	HM2	$4.37 \times 10^{-3}$	$2.86 \times 10^{-1}$	$1.39 \times 10^{-1}$	$2.39 \times 10^{-1}$	$2.21 \times 10^{-5}$	$5.58 \times 10^{-4}$	$4.21 \times 10^{-3}$	$3.11 \times 10^{-1}$	$4.35 \times 10^{-3}$	2.19	$9.98 \times 10^{-2}$
Modified IEEE 123 test feeders	P-lossy [34]	$2.50 \times 10^{-5}$	$3.49 \times 10^{-5}$	$5.40 \times 10^{-4}$	$6.11 \times 10^{-4}$	$1.19 \times 10^{-9}$	$3.60 \times 10^{-8}$	$2.55 \times 10^{-5}$	$1.89 \times 10^{-3}$	$6.52 \times 10^{-3}$	1.03	$5.61 \times 10^{-2}$
	HM2	$2.99 \times 10^{-5}$	$2.58 \times 10^{-4}$	$1.93 \times 10^{-3}$	$8.94 \times 10^{-4}$	$1.73 \times 10^{-4}$	$1.53 \times 10^{-3}$	$2.96 \times 10^{-5}$	$2.08 \times 10^{-3}$	$6.52 \times 10^{-3}$	1.04	$5.81 \times 10^{-2}$

TABLE VIII  
 $\hat{\epsilon}^{\max}$  FOR DIFFERENT MODELS UNDER STOCHASTIC LINE CONDUCTORS IN AC AND DC SUB-NETWORKS

Case name	Model	$\hat{\epsilon}^{\max}$										
		$\tilde{U}_{AC}$	$\theta_{AC}$	$\tilde{P}_{AC}$	$\tilde{Q}_{AC}$	$\tilde{U}_{DC}$	$\tilde{P}_{DC}$	$\tilde{U}_{VSC}$	$\theta_{VSC}$	$\tilde{P}_{VSC}$	$\tilde{Q}_{VSC}$	$\tilde{PL}_{VSC}$
Modified IEEE 33 test feeders	P-lossy [34]	$8.74 \times 10^{-4}$	$2.82 \times 10^{-1}$	$5.09 \times 10^{-1}$	$7.60 \times 10^{-1}$	$4.91 \times 10^{-11}$	$9.11 \times 10^{-10}$	$8.71 \times 10^{-3}$	$3.03 \times 10^{-1}$	$1.56 \times 10^{-3}$	3.67	$9.92 \times 10^{-2}$
	HM2	$7.61 \times 10^{-3}$	$4.43 \times 10^{-1}$	$6.03 \times 10^{-1}$	$9.46 \times 10^{-1}$	$2.82 \times 10^{-5}$	$1.07 \times 10^{-3}$	$7.28 \times 10^{-3}$	$4.60 \times 10^{-1}$	$7.12 \times 10^{-3}$	3.7	$1.73 \times 10^{-1}$
Modified IEEE 123 test feeders	P-lossy [34]	$6.05 \times 10^{-5}$	$8.68 \times 10^{-5}$	$2.37 \times 10^{-3}$	$3.03 \times 10^{-3}$	$5.33 \times 10^{-9}$	$9.21 \times 10^{-8}$	$6.05 \times 10^{-5}$	$4.26 \times 10^{-3}$	$1.59 \times 10^{-2}$	2.74	$5.67 \times 10^{-2}$
	HM2	$6.97 \times 10^{-5}$	$4.71 \times 10^{-4}$	$6.97 \times 10^{-3}$	$3.12 \times 10^{-3}$	$2.81 \times 10^{-4}$	$3.19 \times 10^{-3}$	$6.97 \times 10^{-5}$	$4.61 \times 10^{-3}$	$1.59 \times 10^{-2}$	2.77	$1.45 \times 10^{-1}$

## V. CONCLUSION

In this paper, we revisit the E-lossy models and reformulate a fixed-point iteration problem related to node power injections. The novel fixed-point iteration uses the losses of the next iteration in advance to modify the power injection instead of the current approximated losses.

The proposed lossy power flow model is highly compatible with the characteristics of the distribution network and effectively reduces the computational complexity. Different test cases are used to validate the advantages of the proposed model in pure AC and DC sub-networks, including computational accuracy and convergence performance. Furthermore, we extend the lossy power flow model to hybrid AC-DC distribution networks with VSC. Therefore, we propose a rigorous LPF model based on the complete AC circuit of VSC and formulate a fixed-point iteration model for the lossy power flow of VSC. The results show that the proposed model better approximates the actual operating state of VSCs in MT-interconnected distribution networks. Finally, the performance of the proposed model in face of uncertainty is discussed in two test cases, further proving the greater generality and stability of the proposed model. Future research aims to integrate the technique into the field of hybrid distribution network optimization, e.g., providing efficient and high-quality solutions for expansion planning and operation scheduling.

## REFERENCES

- [1] R. Yang, G. Shi, X. Cai *et al.*, "Autonomous synchronizing and frequency response control of multi-terminal DC systems with wind farm integration," *IEEE Transactions on Sustainable Energy*, vol. 11, no. 4, pp. 2504-2514, Oct. 2020.
- [2] Q. Li and N. Zhao, "General power flow calculation for multi-terminal HVDC system based on sensitivity analysis and extended AC

- grid," *IEEE Transactions on Sustainable Energy*, vol. 13, no. 4, pp. 1886-1899, Oct. 2022.
- [3] D. Boroyevich, I. Cvetković, D. Dong *et al.*, "Future electronic power distribution systems: a contemplative view," in *Proceedings of 2010 12th International Conference on Optimization of Electrical and Electronic Equipment*, Brasov, Romania, May 2010, pp. 1369-1380.
- [4] T. Hakala, T. Lähdeaho, and P. Järventausta, "Low-voltage DC distribution-utilization potential in a large distribution network company," *IEEE Transactions on Power Delivery*, vol. 30, no. 4, pp. 1694-1701, Aug. 2015.
- [5] S. Fu, Y. Gao, X. Chen *et al.*, "Research and project practice on AC and DC distribution network based on flexible substations," *Electric Power Construction*, vol. 39, no. 5, pp. 46-55, May 2018.
- [6] X. Wei, C. Zhang, R. Liu *et al.*, "Key technology breakthrough and demonstration of Suzhou medium and low voltage DC power distribution and consumption system," *Distribution & Utilization*, vol. 39, no. 8, pp. 47-57, Aug. 2022.
- [7] J. Beerten, S. Cole, and R. Belmans, "Generalized steady-state VSC MTDC model for sequential AC-DC power flow algorithms," *IEEE Transactions on Power Systems*, vol. 27, no. 2, pp. 821-829, May 2012.
- [8] J.-C. Fernandez-Perez, F. M. E. Cerezo, and L. R. Rodriguez, "On the convergence of the sequential power flow for multiterminal VSC AC-DC systems," *IEEE Transactions on Power Systems*, vol. 33, no. 2, pp. 1768-1776, Mar. 2018.
- [9] M. A. Allam, A. A. Hamad, and M. Kazerani, "A sequence-component-based power-flow analysis for unbalanced droop-controlled hybrid AC-DC microgrids," *IEEE Transactions on Sustainable Energy*, vol. 10, no. 3, pp. 1248-1261, Jul. 2019.
- [10] Y. Zhang, X. Meng, A. M. Shotorbani *et al.*, "Minimization of AC-DC grid transmission loss and DC voltage deviation using adaptive droop control and improved AC-DC power flow algorithm," *IEEE Transactions on Power Systems*, vol. 36, no. 1, pp. 744-756, Jan. 2021.
- [11] M. Baradar and M. Ghandhari, "A multi-option unified power flow approach for hybrid AC-DC grids incorporating multi-terminal VSC-HVDC," *IEEE Transactions on Power Systems*, vol. 28, no. 3, pp. 2376-2383, Aug. 2013.
- [12] R. Chai, B. Zhang, J. Dou *et al.*, "Unified power flow algorithm based on the NR method for hybrid AC-DC grids incorporating VSCs," *IEEE Transactions on Power Systems*, vol. 31, no. 6, pp. 4310-4318, Nov. 2016.
- [13] S. Khan and S. Bhowmick, "A generalized power-flow model of VSC-based hybrid AC-DC systems integrated with offshore wind farms," *IEEE Transactions on Sustainable Energy*, vol. 10, no. 4, pp. 1775-

- 1783, Oct. 2019.
- [14] E. Aprilia, K. Meng, M. A. Hosani *et al.*, "Unified power flow algorithm for standalone AC-DC hybrid microgrids," *IEEE Transactions on Smart Grid*, vol. 10, no. 1, pp. 639-649, Jan. 2019.
- [15] F. Bizzarri, D. del Giudice, D. Linaro *et al.*, "Partitioning-based unified power flow algorithm for mixed MTDC/AC power systems," *IEEE Transactions on Power Systems*, vol. 36, no. 4, pp. 3406-3415, Jul. 2021.
- [16] J. Yang, N. Zhang, C. Kang *et al.*, "A state-independent linear power flow model with accurate estimation of voltage magnitude," *IEEE Transactions on Power Systems*, vol. 32, no. 5, pp. 3607-3617, Sept. 2017.
- [17] Z. Yuan, Y. Wang, Y. Yi *et al.*, "Fast linear power flow algorithm for the study of steady-state performance of DC grid," *IEEE Transactions on Power Systems*, vol. 34, no. 6, pp. 4240-4248, Nov. 2019.
- [18] Z. Yang, K. Xie, J. Yu *et al.*, "A general formulation of linear power flow models: basic theory and error analysis," *IEEE Transactions on Power Systems*, vol. 34, no. 2, pp. 1315-1324, Mar. 2019.
- [19] Z. Shao, Q. Zhai, Y. Mao *et al.*, "A method for evaluating and improving linear power flow models in system with large fluctuations," *International Journal of Electrical Power & Energy Systems*, vol. 145, p. 108635, Feb. 2023.
- [20] C. Coffrin and P. van Hentenryck, "A linear-programming approximation of AC power flows," *INFORMS Journal on Computing*, vol. 26, no. 4, pp. 718-734, Nov. 2014.
- [21] M. E. Ison and R. Caire, "Commercial linear programming solvers and their applications to power system optimization," in *Proceedings of 2008 IEEE PES General Meeting*, Pittsburgh, USA, Jul. 2008, pp. 1-7.
- [22] Z. Yang, P. Yong, and M. Xiang, "Revisit power system dispatch: concepts, models, and solutions," *iEnergy*, vol. 2, no. 1, pp. 43-62, Mar. 2023.
- [23] B. Stott, J. Jardim, and O. Alsac, "DC power flow revisited," *IEEE Transactions on Power Systems*, vol. 24, no. 3, pp. 1290-1300, Aug. 2009.
- [24] Y. Qi, D. Shi, and D. Tylavsky, "Impact of assumptions on DC power flow model accuracy," in *Proceedings of 2012 North American Power Symposium (NAPS)*, Champaign, USA, Sept. 2012, pp. 1-6.
- [25] S. M. Fatemi, S. Abedi, G. B. Gharehpetian *et al.*, "Introducing a novel DC power flow method with reactive power considerations," *IEEE Transactions on Power Systems*, vol. 30, no. 6, pp. 3012-3023, Nov. 2015.
- [26] J. W. Simpson-Porco, "Lossy DC power flow," *IEEE Transactions on Power Systems*, vol. 33, no. 3, pp. 2477-2485, May 2018.
- [27] C. Coffrin, P. van Hentenryck, and R. Bent, "Approximating line losses and apparent power in AC power flow linearizations," in *Proceedings of 2012 IEEE PES General Meeting*, San Diego, USA, Jul. 2012, pp. 1-8.
- [28] D. Yu, J. Cao, and X. Li, "Review of power system linearization methods and a decoupled linear equivalent power flow model," in *Proceedings of 2018 International Conference on Electronics Technology (ICET)*, Chengdu, China, May 2018, pp. 232-239.
- [29] F. Neumann, V. Hagenmeyer, and T. Brown, "Assessments of linear power flow and transmission loss approximations in coordinated capacity expansion problems," *Applied Energy*, vol. 314, p. 118859, May 2022.
- [30] S. Li, Y. Zhang, and X. Gu, "Skeleton network optimization based on cascade flow method and margin linearization AC power flow model," *Power System Technology*, vol. 47, no. 7, pp. 2788-2798, Jul. 2023.
- [31] M. Marković and B.-M. Hodge, "Parameterized linear power flow for high fidelity voltage solutions in distribution systems," *IEEE Transactions on Power Systems*, vol. 38, no. 5, pp. 4391-4403, Sept. 2023.
- [32] T. Yang, Y. Guo, L. Deng *et al.*, "A linear branch flow model for radial distribution networks and its application to reactive power optimization and network reconfiguration," *IEEE Transactions on Smart Grid*, vol. 2, no. 3, pp. 2027-2036, May 2020.
- [33] J. Zhai, X. Dai, Y. Jiang *et al.*, "Distributed optimal power flow for VSC-MTDC meshed AC-DC grids using ALADIN," *IEEE Transactions on Power Systems*, vol. 37, no. 6, pp. 4861-4873, Nov. 2022.
- [34] J.-C. Fernandez-Perez, F. M. E. Cerezo, and L. R. Rodriguez, "Linear power flow algorithm with losses for multi-terminal VSC AC-DC power systems," *IEEE Transactions on Power Systems*, vol. 37, no. 3, pp. 1739-1749, May 2022.
- [35] T. Zhang, Y. Mu, J. Zhao *et al.*, "Distributed OPF for PET-based AC-DC distribution networks with convex relaxation and linear approximation," *IEEE Transactions on Smart Grid*, vol. 13, no. 6, pp. 4340-4354, Nov. 2022.
- [36] X. He, T. Ding, Y. Sun *et al.*, "Interval reliability evaluation of hybrid AC/DC grids with integrated renewable energy," *IEEE Transactions on Power Systems*, vol. 28, no. 5, pp. 4501-4514, Sept. 2023.
- [37] L. Zhang, B. Zhang, W. Tang *et al.*, "A coordinated restoration method of hybrid AC-DC distribution network with electric buses considering transportation system influence," *IEEE Transactions on Industrial Informatics*, vol. 18, no. 11, pp. 8236-8246, Nov. 2022.
- [38] H. Ergun, J. Dave, D. van Hertem *et al.*, "Optimal power flow for AC-DC grids: formulation, convex relaxation, linear approximation, and implementation," *IEEE Transactions on Power Systems*, vol. 34, no. 4, pp. 2980-2990, Jul. 2019.
- [39] J. S. Giraldo, P. P. Vergara, J. C. López *et al.*, "A linear AC-OPF formulation for unbalanced distribution networks," *IEEE Transactions on Industry Applications*, vol. 57, no. 5, pp. 4462-4472, Sept.-Oct. 2021.
- [40] Z. Li, J. Yu, and Q.-H. Wu, "Approximate linear power flow using logarithmic transform of voltage magnitudes with reactive power and transmission loss consideration," *IEEE Transactions on Power Systems*, vol. 33, no. 4, pp. 4593-4603, Jul. 2018.
- [41] R. D. Zimmerman, C. E. Murillo-Sanchez, and R. J. Thomas, "MATPOWER: steady-state operations, planning, and analysis tools for power systems research and education," *IEEE Transactions on Power Systems*, vol. 26, no. 1, pp. 12-19, Feb. 2011.

**Hao Wang** received the M. S. degree from Northeastern University, Shenyang, China, in 2021. He is currently working toward the Ph.D. degree with the School of Electrical Engineering, Chongqing University, Chongqing, China. His current research interests include modelling and optimization of integrated transmission and distribution systems.

**Changzheng Shao** received the B.S. degree in electrical engineering from Shandong University, Jinan, China, and the Ph.D. degree in electrical engineering from Zhejiang University, Hangzhou, China, in 2015 and 2020, respectively. He is currently an Assistant Professor with Chongqing University, Chongqing, China. His research interests include operation optimization and reliability evaluation of integrated energy system.

**Yu Wang** received the M.Sc. and Ph.D. degrees in power engineering from Nanyang Technological University, Singapore, in 2012 and 2017, respectively. Currently, he is a Professor at the School of Electrical Engineering, Chongqing University, Chongqing, China. His research interests include microgrid control and stability, power system operation and control, and cyber-physical system.

**Bo Hu** received the received the Ph.D. degree in electrical engineering from Chongqing University, Chongqing, China, in 2010. He is currently working as a Full Professor with the School of Electrical Engineering, Chongqing University. His research interests include power system reliability and parallel computing technique in power system.

**Kaigui Xie** received the Ph.D. degree in power system and its automation from Chongqing University, Chongqing, China, in 2001. He is a currently a Full Professor with the School of Electrical Engineering, Chongqing University. His research interests include power system reliability, planning, and analysis.

**Pierluigi Siano** received the M.Sc. degree in electronic engineering and the Ph.D. degree in information and electrical engineering from the University of Salerno, Salerno, Italy, in 2001 and 2006, respectively. He is a Professor and Scientific Director of the Smart Grids and Smart Cities Laboratory with the Department of Management and Innovation Systems, University of Salerno. His research interests include integration of distributed energy resources in smart grid, and planning and management of power system.